3-24-2020

CD137 signaling regulates acute colitis via RALDH2-expressing CD11b−CD103+ DCs

Jing Jin

In-Hyuk Jung

Se-Jin Jeong

et al

Article

Cell Reports

CD137 Signaling Regulates Acute Colitis via RALDH2-Expressing CD11b^{-}CD103^{+} DCs

Graphical Abstract

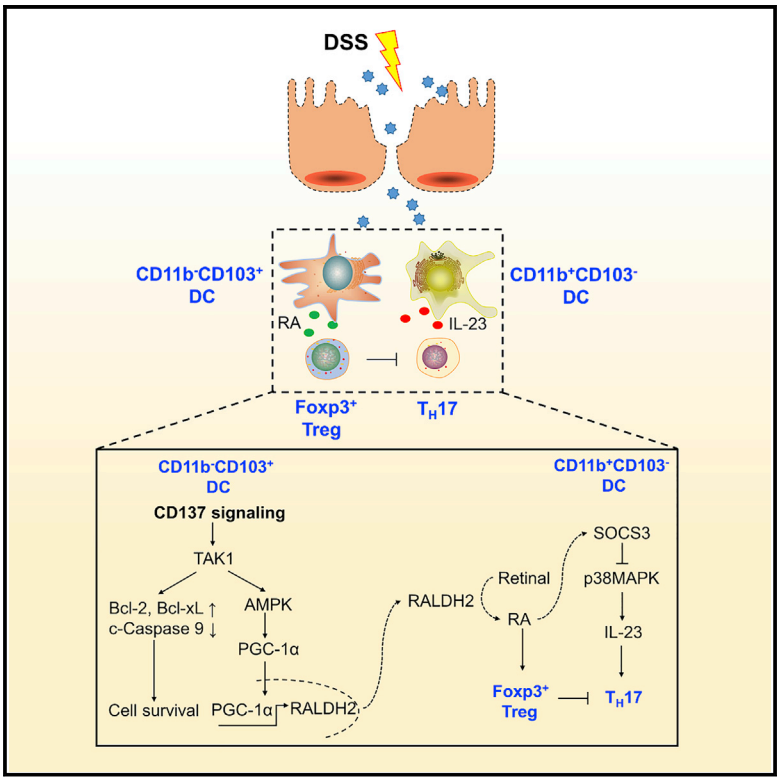

Highlights

- CD137 signaling is critical for the survival of CD11b^{-}CD103^{+} DCs during colitis
- The CD137-activated TAK1-AMPK-PGC-1α axis increases retinoic acid (RA) production
- RA acts on CD11b^{+}CD103^{-} DCs to inhibit IL-23 production in a paracrine manner
- CD137 signaling slows down acute colitis progression

Authors

Jing Jin, In-Hyuk Jung, Shin Hye Moon, ..., Jae-Hoon Choi, Byungsuk Kwon, Goo Taeg Oh

Correspondence

bkwon@ulsan.ac.kr (B.K.), gootaeg@ewha.ac.kr (G.T.O.)

In Brief

Jin et al. demonstrate that CD137 signaling functions as an immune checkpoint by controlling the survival and function of regulatory intestinal CD11b^{-}CD103^{+} dendritic cells to coordinate the balance between regulatory T cells and pathogenic IL-23 during acute colitis.

Jin et al., 2020, Cell Reports *30*, 4124–4136
March 24, 2020
https://doi.org/10.1016/j.celrep.2020.02.103

CellPress

OPEN ACCESS
CellPress

Cell Reports
Article

CD137 Signaling Regulates Acute Colitis via RALDH2-Expressing CD11b^{-}CD103^{+} DCs

Jing Jin,[1] In-Hyuk Jung,[2] Shin Hye Moon,[1] Sejin Jeon,[1] Se-Jin Jeong,[2] Seong-Keun Sonn,[1] Seungwoon Seo,[1] Mi-Ni Lee,[1] Eun Ju Song,[1] Hyae Yon Kweon,[1] Sinai Kim,[1] Tae Kyeong Kim,[1] Juyang Kim,[3] Hong Rae Cho,[4] Jae-Hoon Choi,[5] Byungsuk Kwon,[3,*] and Goo Taeg Oh[1,6,*]

[1]Immune and Vascular Cell Network Research Center, National Creative Initiatives, Department of Life Sciences, Ewha Womans University, Seoul 120-750, South Korea
[2]Cardiovascular Division, Department of Medicine, Washington University School of Medicine, St. Louis, MO 63110, USA
[3]School of Biological Sciences and Biomedical Research Center, University of Ulsan, Ulsan 44610, South Korea
[4]Department of Surgery and Biomedical Research Center, Ulsan University Hospital, College of Medicine, University of Ulsan, Ulsan 44610, South Korea
[5]Department of Life Science, College of Natural Sciences, Research Institute for Natural Sciences, Hanyang University, Seoul 133-791, South Korea
[6]Lead Contact
*Correspondence: bkwon@ulsan.ac.kr (B.K.), gootaeg@ewha.ac.kr (G.T.O.)
https://doi.org/10.1016/j.celrep.2020.02.103

SUMMARY

CD137, a potent costimulatory receptor for CD8^{+} T cells, is expressed in various non-T cells, but little is known about its regulatory functions in these cells. In this study, we show that CD137 signaling, specifically in intestinal CD11b^{-}CD103^{+} dendritic cells (DCs), restricts acute colitis progression. Mechanistically, CD137 engagement activates TAK1 and subsequently stimulates the AMPK-PGC-1α axis to enhance expression of the *Aldh1a2* gene encoding the retinoic acid (RA) metabolizing enzyme RALDH2. RA can act on CD11b^{+}CD103^{-} DCs and induce SOCS3 expression, which, in turn, suppresses p38MAPK activation and interleukin-23 (IL-23) production. Administration of RA in DC-specific *CD137*$^{-/-}$ mice represses IL-23-producing CD11b^{+}CD103^{-} DCs and T_H17 cells, indicating that RA is a major inhibitory effector molecule against intestinal CD11b^{+}CD103^{-} DCs. Additionally, the therapeutic effect of the anti-CD137 antibody is abrogated in DC-specific *CD137*$^{-/-}$ mice. Taken together, our results define a mechanism of paracrine immunoregulation operating between adjacent DC subsets in the intestine.

INTRODUCTION

CD137 (also known as 4-1BB and TNFRSF9) and its ligand, CD137L (also called 4-1BBL or TNFSF9), are expressed on a variety of hematopoietic and non-hematopoietic cells, where their expression is mostly inducible (Lee and Croft, 2009). Early studies showed that CD137 functions as a potent costimulatory receptor for CD8^{+} T cells (Melero et al., 1997; Shuford et al., 1997), but more recent reports have extended its functions beyond lymphoid cells (Hsieh et al., 2010; Jeon et al., 2010; Kim et al., 2012; Nishimoto et al., 2005). Due to the existence of CD137L reverse signaling, which plays a critical role in the immune response (Jeon et al., 2010; Kang et al., 2017; Langstein et al., 1998; Schwarz, 2005; Kim et al., 2012), findings regarding the functions of CD137 should be interpreted with a degree of caution. Indeed, CD137 and CD137L are likely to have coevolved to fulfill the same purpose (Kwon, 2012): their bidirectional signaling pathways cooperate in multiple phases of the immune response, including acute inflammation, inflammation resolution, and even the dysregulation of chronic inflammation (Eun et al., 2015; Jeon et al., 2010; Kang et al., 2017; Mak et al., 2019). Given this, the spatiotemporal pairing of CD137- or CD137L-expressing cells should be finely tuned during each step of an inflammatory process. Interestingly, the CD137-CD137L system functions as an immune checkpoint at the phase of dendritic cell (DC) differentiation (Lee et al., 2008, 2012; Kang et al., 2017; Kwon, 2018). For example, CD137 signaling triggers the production of retinoic acid (RA) by CD103^{+} DCs in the gut-associated lymphoid organs, which, in turn, generates inducible Foxp3^{+} regulatory T (iTreg) cells (Lee et al., 2012). On the other hand, CD137L signaling creates an anti-inflammatory environment within tumors by inhibiting the differentiation of interleukin (IL)-12-producing CD103^{+} DCs while promoting that of CD11b^{+} DCs (Kang et al., 2017). However, little is known regarding how CD137 signaling in DCs regulates acute inflammation.

DCs play a pivotal role in maintaining intestinal homeostasis and curbing the inflammation caused by the multilayered disruption of intestinal homeostasis. The conventional DCs found in the intestine can be broadly divided into two major subsets: CD103^{+} cDC1s and CD11b^{+} cDC2s (Guilliams et al., 2014). The cDC2s can be further classified into CD103^{+} and CD103^{-} fractions, which dominate in the small intestine and the colon, respectively (Bogunovic et al., 2009; Satpathy et al., 2013). The diversification of DCs, which is determined during the common DC progenitor stage in the bone marrow (Grajales-Reyes et al., 2015; Schlitzer et al., 2015), allows for specialization in effective immunity and tolerance. For example, CD103^{+} cDCs are required for the inductions of T helper 1 (T_H1) and Treg cells, whereas CD11b^{+} cDCs are critical for the induction of T_H2 cells, T_H17 cells, and T follicular helper (T_{FH}) cells (Durai and Murphy, 2016). Although the functional dichotomy is

less well understood in intestinal DCs, it is thought that intestinal $CD103^+$ cDC1s and intestinal $CD11b^+CD103^+$ DC2s are preferentially required for the differentiation of Treg cells and T_H17 cells, respectively (Joeris et al., 2017).

Dextran sodium sulfate (DSS) is commonly used to induce acute colitis in model animals (Kiesler et al., 2015; Eichele and Kharbanda, 2017). A decade ago, DCs were shown to be positively or negatively involved in the development of DSS-induced acute colitis (Abe et al., 2007; Berndt et al., 2007), but little is known regarding how these processes are regulated. A recent study demonstrated that p38α inhibits the TAK1-MKK4/7-JNK-IL-27 axis in intestinal $CD103^+$ DC1s and thereby decreases the generation of type 1 Treg (Tr1) cells and type 3 innate lymphoid cells (ILC3s) (Zheng et al., 2018). p38α-deficient DC1s direct the differentiation of Tr1 cells and ILC3s via IL-27 production; the respective products of these cells, IL-10 and IL-22, subsequently restrict intestinal inflammation and restore epithelial barrier function, respectively (Zheng et al., 2018). In the present study, we report that TAK1 acts as a divergence point for CD137 signaling in intestinal $CD103^+$ cDCs to regulate acute colitis. It does so by increasing the survival of these cells on one hand and by giving them a tolerogenic capacity through induction of RALDH2 expression on the other hand. The TAK1-AMPK axis stimulates the nuclear translocation of PGC-1α to induce RALDH2 expression; thereafter, RA mediates two important regulatory functions; namely, the generation of Treg cells and the suppression of IL-23 production by $CD11b^+CD103^-$ DCs via induction of SOCS3. Taken together, our results identify CD137 as an immune checkpoint for acute colitis, which has therapeutic implications for inflammatory bowel disease.

RESULTS

CD137$^{-/-}$ Mice Exhibit Increased Susceptibility to Acute Colitis

Colitis is known to be uncontrollable in *CD137*$^{-/-}$ mice (Martínez Gómez et al., 2013), but the mechanism underlying this process remains to be clarified. In our experiments, mice were given 2% DSS in the drinking water *ad libitum* for 9 days. There was a progressive body weight loss from day 5 to day 9 in both wild-type (WT; *CD137*$^{+/+}$) and *CD137*$^{-/-}$ mice, with a significantly greater reduction rate seen in *CD137*$^{-/-}$ mice (Figure 1A). Consistently, *CD137*$^{-/-}$ mice exhibited greater shortening of the colon length (Figure 1B). Histological and immunohistochemical analyses demonstrated more distinguishable differences, including more severe inflammation and tissue damage with loss of epithelial crypts, in *CD137*$^{-/-}$ mice compared to WT mice (Figures 1C–1E). Interestingly, however, there was no difference in the severity of colitis in *CD137L*$^{+/+}$ versus *CD137L*$^{-/-}$ mice (Figure S1).

CD137$^{-/-}$ Mice Have a Decreased Frequency of Intestinal $CD11b^-CD103^+$ DCs and $Foxp3^+$ Treg Cells during Acute Colitis

To define characteristic changes in the intestine of *CD137*$^{-/-}$ mice, we analyzed the composition of intestinal immune cells in the lamina propria (LP) and mesenteric lymph nodes (MLNs) on day 9. By adopting a strict gating strategy for the $CD45^+$ LP leukocyte pool, we identified $CD11b^+Ly6G^+$ cells as neutrophils and $Ly6G^-CD11b^+F4/80^+$ cells as macrophages. After further excluding $CD11b^+Ly6C^{hi}$ monocytes, we gated $CD11c^+MHCII^+$ from the remaining cells as DCs (Figure S2A). The obtained DCs were subdivided into four groups based on the expression of CD11b and/or CD103 (Figure S2A). We further defined $CD11b^+Ly6C^{hi}$ monocytes as $CX3CR1^{int}MHCII^{lo}CCR2^{hi}$ cells and $CD11b^+F4/80^+$ macrophages as $CX3CR1^{hi}MHCII^+CCR2^{lo}$ cells (Figure S2B). Unlike DCs, macrophages expressed CD64 (Figure S2B) and showed a higher phagocytic activity (Figure S2C), confirming that the purified $CD11b^+CD103^-$ DCs were genuine DCs. Surprisingly, WT and *CD137*$^{-/-}$ mice had no difference in the frequency of neutrophils, macrophages, monocytes, or DCs among the $CD45^+$ leukocytes of the LP (Figure S2D). We also observed the same pattern of immune cell composition in the MLNs (Figure S2E). However, there was a lower frequency of $CD11b^-CD103^+$ DC subsets among the $CD45^+$ leukocyte populations in the LP and MLNs of *CD137*$^{-/-}$ mice versus WT mice, with the opposite pattern seen for $CD11b^+CD103^-$ DCs (Figures 2A and 2B). In a steady state, there was no difference in the frequency of DC subsets in the LP of WT versus *CD137*$^{-/-}$ mice (Figure S3A). In addition, WT and *CD137*$^{-/-}$ mice had no quantitative difference in the frequency of LP pre-DCs or that of DC progenitors in the bone marrow (BM) (Figures S3B and S3C). These results indicate that CD137 signaling played a major role in the process of DC maturation toward $CD11b^-CD103^+$ DCs during acute colitis.

We observed a lower activity of retinaldehyde dehydrogenase 2 (RALDH2, an enzyme involved in the production of RA in DCs) in *CD137*$^{-/-}$ LP and MLN $CD11b^-CD103^+$ DCs (Figures 2C and 2D) but not in $CD11b^+CD103^-$ DCs (Figures 2E and 2F). Consistent with previous studies (Lee et al., 2012), $CD137^+CD11b^-CD103^+$ DCs exhibited higher RALDH2 activity (Figure 2G). There was no difference in the RALDH2 activity of macrophages, another major producer of RA (Broadhurst et al., 2012), in *CD137*$^{-/-}$ versus WT LP and MLN $CD11b^-CD103^+$ DCs (Figures S3D and S3E). Another regulatory effector molecule produced by cDC1s is IL-27, which regulates T_r1 differentiation (Zheng et al., 2018). However, we did not observe any difference in intracellular levels of IL-27 of intestinal $CD11b^-CD103^+$ DCs between WT and *CD137*$^{-/-}$ mice (Figures S3F and S3G). As $CD11b^-CD103^+$ DCs have the unique ability to induce Treg cells in the intestine (Izcue et al., 2006; Sun et al., 2007), a reduction in their frequency might be associated with a lower frequency of Treg cells and more severe colitis. *CD137*$^{-/-}$ mice had a higher number of $CD4^+$ T cells in the LP (Figure 2H) and an increased frequency of these cells in MLNs (Figure 2I). Importantly, the frequency of Treg cells was decreased in the LP and MLNs of *CD137*$^{-/-}$ mice (Figure 2J), even though the percentage of LP and MLN iTreg cells showed no difference between the two groups (Figure S3H). Taken together, our results suggest that quantitative and qualitative changes in intestinal $CD11b^-CD103^+$ DCs may underlie the impaired ability of *CD137*$^{-/-}$ mice to regulate intestinal inflammation.

CD137 Signaling in DCs Is Critical for Regulating Acute Colitis

Consistent with the observation that numerical and functional changes of LP and MLN $CD11b^-CD103^+$ DCs were a

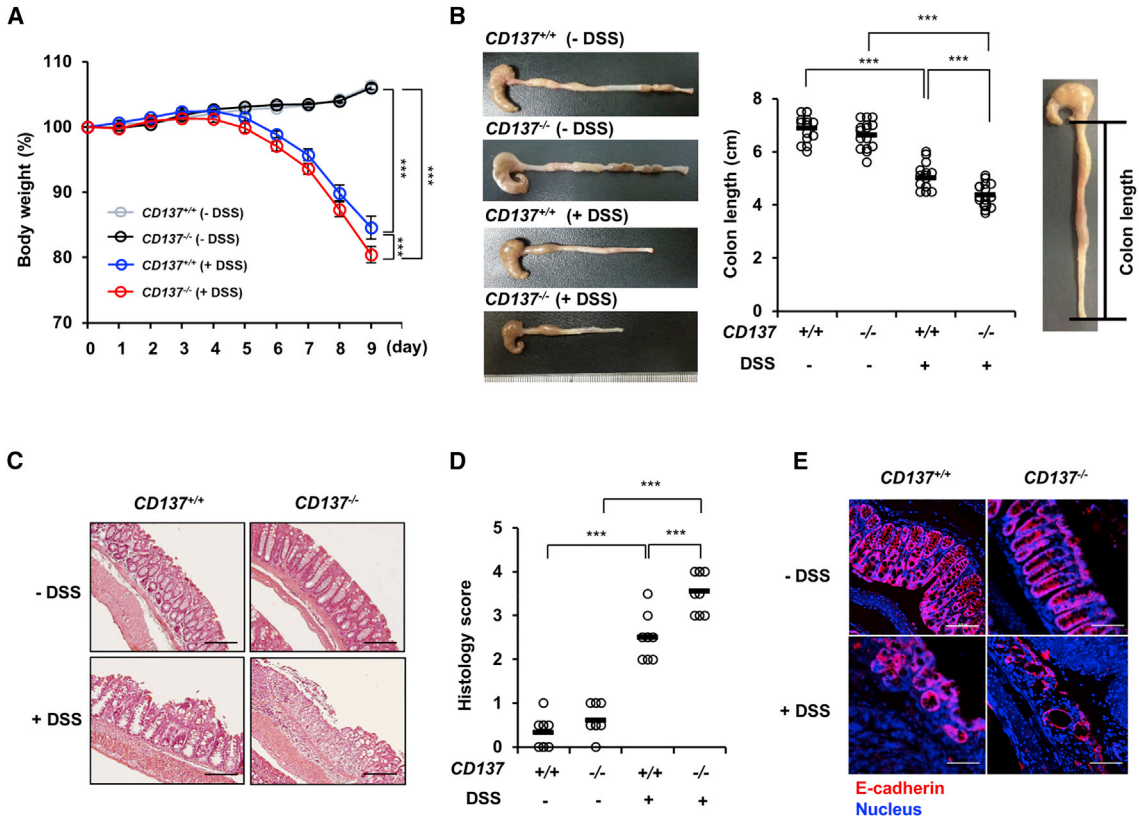

Figure 1. CD137 Deficiency Promotes Acute Colitis

(A) Body weight changes of $CD137^{+/+}$ (noncolitic, n = 10), $CD137^{-/-}$ (noncolitic, n = 10), $CD137^{+/+}$ (colitic, n = 10), and $CD137^{-/-}$ (colitic, n = 10) mice. Data were presented as mean ± SEM. ***p < 0.001 (Student's t test).

(B) Colon length of $CD137^{+/+}$ (noncolitic, n = 13), $CD137^{-/-}$ (noncolitic, n = 15), $CD137^{+/+}$ (colitic, n = 13), and $CD137^{-/-}$ (colitic, n = 14) mice. ***p < 0.001 (Student's t test).

(C) Representative microscopic images of H&E-stained colon sections of $CD137^{+/+}$ (noncolitic), $CD137^{-/-}$ (noncolitic), $CD137^{+/+}$ (colitic), and $CD137^{-/-}$ (colitic) mice. Scale bars, 100 μm.

(D) Crypt damage scores of $CD137^{+/+}$ (noncolitic, n = 8), $CD137^{-/-}$ (noncolitic, n = 8), $CD137^{+/+}$ (colitic, n = 8), and $CD137^{-/-}$ (colitic, n = 8) mice. ***p < 0.001 (Student's t test).

(E) Representative microscopic images of immunofluorescence-stained colon sections of $CD137^{+/+}$ (noncolitic), $CD137^{-/-}$ (noncolitic), $CD137^{+/+}$ (colitic), and $CD137^{-/-}$ (colitic) mice. Scale bars, 100 μm. ***p < 0.001 (Student's t test).

See also Figure S1.

distinguishable feature of $CD137^{-/-}$ mice with acute colitis, CD137 expression in LP CD11b^{-}CD103^{+} DCs was the most prominent, and its upregulation was also marked during colitis in this subset (Figures 3A and 3B). We next explored whether the disease phenotype observed in $CD137^{-/-}$ mice would be reproduced in $CD11c^{Cre}CD137^{fl/fl}$ mice. We included $CD137^{fl/fl}$ and $Lyz2^{Cre}CD137^{fl/fl}$ mice as controls. CD137 expression was confirmed to be markedly reduced in DCs and macrophages of $CD11c^{Cre}CD137^{fl/fl}$ and $Lyz2^{Cre}CD137^{fl/fl}$, respectively (Figures S4A–S4D). $CD11c^{Cre}CD137^{fl/fl}$ mice exhibited greater degrees of body weight loss and colon shortening compared to those in both control groups (Figures 3C and 3D). Histological and immunohistochemical analyses demonstrated additional differences, including increased severity of intestinal inflammation and tissue damage with loss of epithelial crypts in $CD11c^{Cre}CD137^{fl/fl}$ mice (Figures 3E and 3F). More importantly, the percentages of LP and MLN CD11b^{-}CD103^{+} DCs were lower in $CD11c^{Cre}CD137^{fl/fl}$ mice versus $CD137^{fl/fl}$ mice (Figures 3G and 3H). It has been reported that CCR7 is critically important in LP DCs for migration to MLNs (Jang et al., 2006). However, CD137 signaling did not seem to be involved in the migration of DCs to the LP, as their cell surface levels of CCR7 were not different between $CD11c^{Cre}CD137^{fl/fl}$ and $CD137^{fl/fl}$ mice (Figures S4E and S4F). Our findings clearly indicate that CD137 signaling in DCs is associated with the maintenance of LP and MLN CD11b^{-}CD103^{+} DCs during acute colitis, which is linked to the proper control of colon inflammation.

CD137 Signaling Regulates the Survival of CD11b^{-}CD103^{+} DCs through TAK1

The epithelial disruption induced by DSS allows Gram-negative bacteria to enter the LP and exacerbates colon inflammation (Figure S5A). To mimic the *in vivo* colitis condition in an *in vitro* system, we examined CD137 signaling in mature CD11b^{-}CD103^{+} DCs in

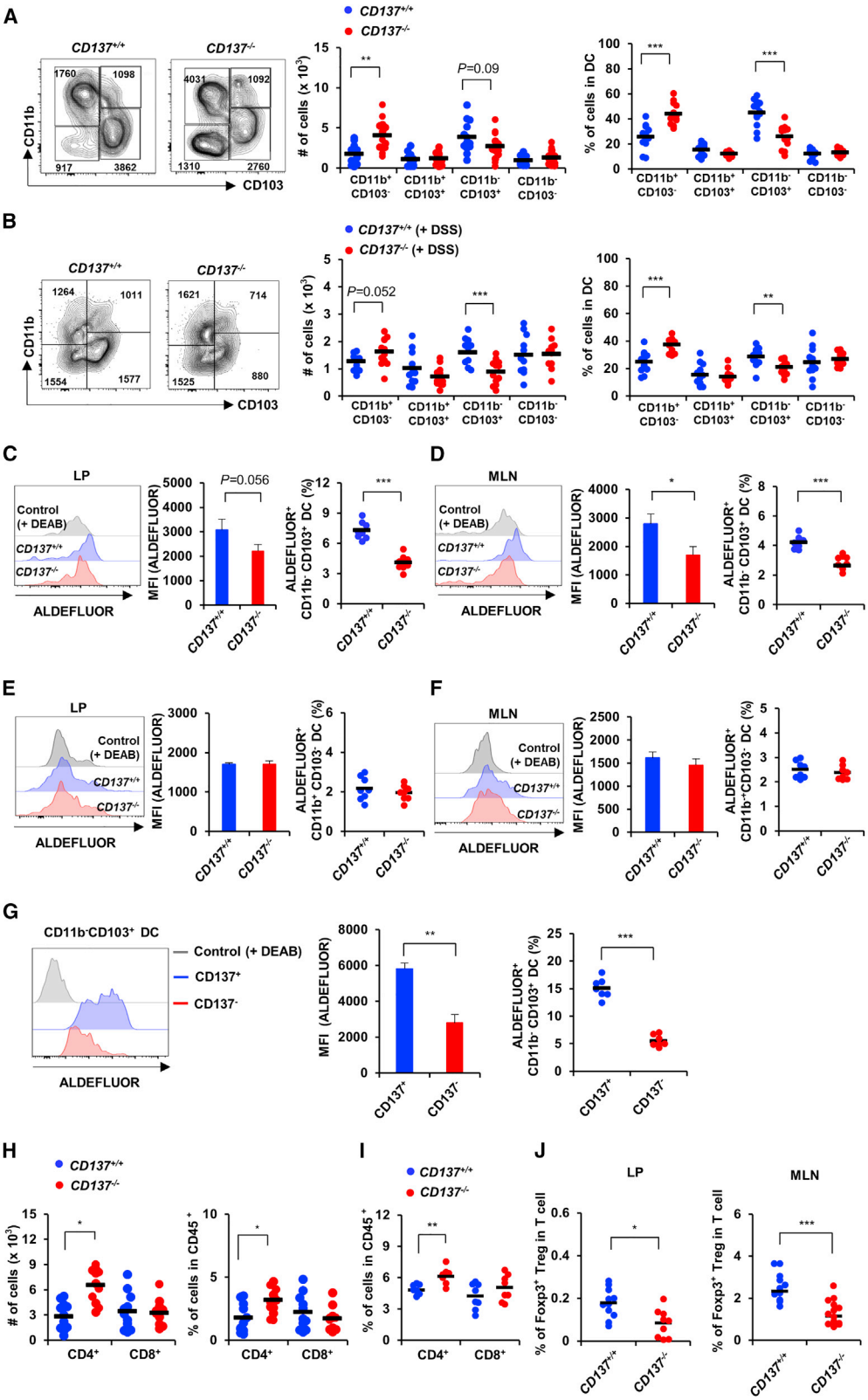

(legend on next page)

the presence of *E. coli* lipopolysaccharide (LPS). BM-derived DCs (BMDCs) were generated from BM cells in the presence of Fms-related tyrosine kinase ligand (Flt3L) for 9 days, and $CD11b^{-}CD103^{+}$ DC polarization was induced by adding interferon gamma (IFN-γ) and granulocyte-macrophage colony-stimulating factor (GM-CSF) for 2 days (Tussiwand et al., 2012; Kang et al., 2017). Approximately 80% of cells were polarized to $CD11b^{-}CD103^{+}$ subsets after IFN-γ and GM-CSF stimulation. However, LPS treatment reduced the portion of $CD11b^{-}CD103^{+}$ cells only in *CD137*$^{-/-}$ DC culture (Figure 4A; Figure S5B), and the percentages of $CD11b^{+}CD103^{-}$ cells were comparable between WT and *CD137*$^{-/-}$ cells (Figures S5B and S5C). This was due to increased apoptosis specific for these cells (Figure 4B). In addition, blocking the CD137 signal transduction pathway with anti-CD137L antibody also induced a reduction in WT $CD11b^{-}CD103^{+}$ DC portions (Figure S5D) and in their *Bcl-2* transcription (Figure S5E). These results may explain the reduction in $CD103^{+}$ DCs in colitic *CD137*$^{-/-}$ mice and human patients with Crohn's disease (Strauch et al., 2010; Magnusson et al., 2016).

Previous studies have demonstrated that CD137 signaling serves as a survival factor in DCs by increasing expression of the anti-apoptotic molecules Bcl-2 and Bcl-xL (Choi et al., 2009). In our *in vitro* experimental system, LPS augmented expression of not only CD137 but also Bcl-2 and Bcl-xL in WT $CD11b^{-}CD103^{+}$ DCs, but inhibition of CD137 signaling by either genetic deletion of CD137 or anti-CD137L antibody failed to enhance expression of Bcl-2 and Bcl-xL in these DCs (Figures 4C–4F; Figure S5E). Consistently, LPS induced the phosphorylation of the p65 subunit of nuclear factor κB (NF-κB) in WT $CD11b^{-}CD103^{+}$ DCs while decreasing cleavage of caspase 9 (Figure 4F). Related to this, we found that the engagement of CD137 with an anti-CD137 agonist (3E1) was particularly effective in modulating the LPS-mediated upregulation of *Bcl-2* and *Bcl-xL* and the inhibition of caspase-9 cleavage in WT DCs but not in *CD137*$^{-/-}$ $CD11b^{-}CD103^{+}$ DCs (Figures 4G and 4H). Notably, the levels of Bcl-2 and cleaved caspase-9 were not influenced by LPS in either WT or *CD137*$^{-/-}$ $CD11b^{+}CD103^{-}$ DCs (Figures S5F–S5H). We also confirmed that the protein levels of Bcl-2 and Bcl-xL were decreased and that those of cleaved caspase-9 were increased in *CD11c*^{Cre}*CD137*$^{fl/fl}$ LP and MLN $CD11b^{-}CD103^{+}$ DCs after colitis induction (Figures 4I–4L).

TAK1 has been shown to be critical for the regulatory activity of DCs (Zheng et al., 2018). Stimulation of CD137 in $CD11b^{-}CD103^{+}$ DCs induced phosphorylation of TAK1, but this did not occur in $CD11b^{-}CD103^{+}$ DCs pretreated with a TAK1 inhibitor (Figures 4M and 4N). Importantly, this inhibitor abolished the LPS-mediated increase in Bcl-2 expression and decrease in cleaved caspase-9 in WT DCs but not in *CD137*$^{-/-}$ $CD11b^{-}CD103^{+}$ DCs (Figure 4O). Taken together, our results suggest that CD137 signaling in $CD11b^{-}CD103^{+}$ DCs specifically regulates their maturation and survival during intestinal inflammation in both transcription-dependent and -independent manners.

The TAK1-AMPK-PGC1α Axis Is Required for the Production of RA by CD137 Signaling

We hypothesized that CD137 signaling results in RA production via TAK1 in $CD11b^{-}CD103^{+}$ DCs. Indeed, our experiments showed that CD137 stimulation increased the expression of *Aldh1a2* (encoding RALDH2 enzyme) in WT but not in *CD137*$^{-/-}$ $CD11b^{-}CD103^{+}$ DCs (Figure 5A). Since AMPK is a kinase downstream of TAK1, we also examined its involvement in CD137 signaling. As expected, stimulation of CD137 with an anti-CD137 antibody increased the phosphorylation level of AMPK and the expression of RALDH2 (Figure 5B). However, TAK1 inhibition completely abrogated the effect of this anti-CD137 antibody (Figure 5B). These results further confirmed that TAK1 is involved in the expression of RALDH2 after CD137 stimulation in $CD11b^{-}CD103^{+}$ DCs.

PGC-1α (encoded by *Ppargc1a*) is a coactivator of many transcription factors; it acts as a substrate for AMPK (Jäger et al., 2007), which also induces increased *Ppargc1a* expression (Lin et al., 2005). Consistent with these observations, CD137 stimulation triggered upregulation of *Ppargc1a* in $CD11b^{-}CD103^{+}$ DCs (Figure 5C) and induced the translocation of the encoded protein into the nucleus (Figure 5D). These activities were abolished by TAK1 inhibition (Figures 5C and 5D).

As RA secreted by DCs has been reported to regulate multiple aspects of immune responses (Manicassamy et al., 2009; Manicassamy and Pulendran, 2009), we next examined whether RA has an immunosuppressive effect on $CD11b^{+}CD103^{-}$ DCs. BMDCs were polarized into $CD11b^{+}CD103^{-}$ DCs following 2 days of supplementation with IL-23 and GM-CSF. Treatment of these $CD11b^{+}CD103^{-}$ DCs with RA increased SOCS3 at the transcriptional and translational levels (Figures 5E and 5F). Decreased phosphorylation of p38MAPK, which is a target of SOCS3, was associated with the RA-mediated induction of SOCS3 (Figure 5F). Consistently, RA inhibited IL-23 expression and secretion by LPS-stimulated $CD11b^{+}CD103^{-}$ DCs (Figures

Figure 2. CD137 Deficiency Decreases $CD11b^{-}CD103^{+}$ DCs and $Foxp3^{+}$ Treg Cells in Acute Colitis

(A and B) Flow-cytometric analysis for LP (A) and MLN (B) DCs of colitic *CD137*$^{+/+}$ mice (n = 13 in LP; n = 12 in MLN) and *CD137*$^{-/-}$ mice (n = 13 in LP; n = 12 in MLN). $^{**}p < 0.01$; $^{***}p < 0.001$ (Student's t test).

(C and D) Flow-cytometric analysis for ALDEFLUOR staining of LP (C) and MLN (D) $CD11b^{-}CD103^{+}$ DCs of colitic *CD137*$^{+/+}$ (n = 8) and *CD137*$^{-/-}$ mice (n = 8). Data are presented as mean ± SEM. $^{*}p < 0.05$; $^{***}p < 0.001$ (Student's t test).

(E and F) Flow-cytometric analysis for ALDEFLUOR staining of LP (E) and MLN (F) $CD11b^{+}CD103^{-}$ DCs of colitic *CD137*$^{+/+}$ (n = 8) and *CD137*$^{-/-}$ mice (n = 8).

(G) Flow-cytometric analysis for ALDEFLUOR staining in $CD137^{+}$ or $CD137^{-}$ LP $CD11b^{-}CD103^{+}$ DCs of colitic *CD137*$^{+/+}$ mice (n = 7). Data are presented as mean ± SEM. $^{**}p < 0.01$; $^{***}p < 0.001$ (Student's t test).

(H) Flow-cytometric analysis for LP $CD4^{+}$ and $CD8^{+}$ T cells of colitic *CD137*$^{+/+}$ (n = 11) and *CD137*$^{-/-}$ mice (n = 11). $^{*}p < 0.05$ (Student's t test).

(I) Flow-cytometric analysis for MLN $CD4^{+}$ and $CD8^{+}$ T cells of colitic *CD137*$^{+/+}$ (n = 8) and *CD137*$^{-/-}$ mice (n = 8). $^{**}p < 0.05$ (Student's t test).

(J) Flow-cytometric analysis for LP and MLN $Foxp3^{+}$ Treg cells of colitic *CD137*$^{+/+}$ (n = 11 in both LP and MLN) and *CD137*$^{-/-}$ mice (n = 9 in LP; n = 14 in MLN). $^{*}p < 0.05$; $^{***}p < 0.001$ (Student's t test).

See also Figures S2 and S3.

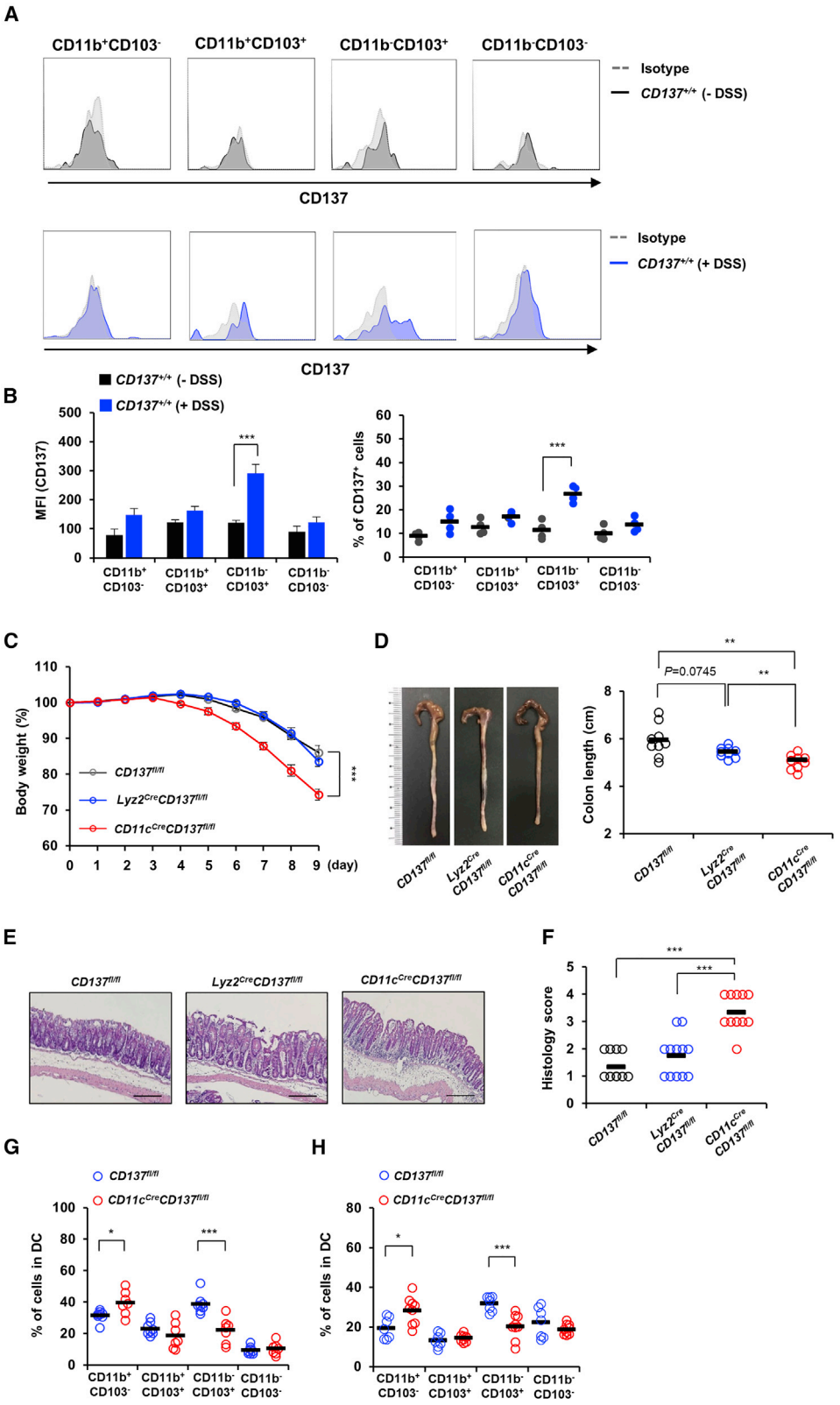

(legend on next page)

5G–5I). Finally, to directly show that RA produced by CD11b^{-}CD103^{+} DCs can suppress IL-23 production of CD11b^{+}CD103^{-} DCs, we co-cultured these two cell types in the Transwell system. CD11b^{+}CD103^{-} DCs were pretreated with RA receptor antagonist and co-cultured with WT or *CD137*$^{-/-}$ CD11b^{-}CD103^{+} DCs under LPS stimulation. We found that the RA receptor antagonist increased IL-23 production of WT CD11b^{+}CD103^{-} DCs but that it did not induce such an increase in the CD11b^{-}CD103^{+} DCs of *CD137*$^{-/-}$ mice (Figures 5J and 5K). Our results indicate that CD11b^{-}CD103^{+} DCs may suppress the immunostimulatory activity of CD11b^{+}CD103^{-} DCs through RA.

CD137 Signaling in CD11b^{-}CD103^{+} DCs Inhibits the Differentiation of T_H17 Cells

CD11b^{+}CD103^{-} DCs are known to promote intestinal inflammation by activating and inducing mucosal T_H17 cell responses through IL-23 (Schlitzer et al., 2013; Scott et al., 2015). Since the frequency of intestinal CD11b^{+}CD103^{-} DCs was increased in *CD137*$^{-/-}$ mice with colitis (Figures 2A and 2B; Figures 3G and 3H), we hypothesized that increased CD11b^{+}CD103^{-} DCs and decreased CD11b^{-}CD103^{+} DCs in the intestine would cause hyper-activated T_H17 cell responses in *CD137*$^{-/-}$ mice. We observed a significantly higher number of effector CD4^{+} T cells in the LP of *CD137*$^{-/-}$ mice (Figure 2H), and their frequency was also greater in the MLNs (Figure 2I). More importantly, *CD137*$^{-/-}$ LP CD11b^{+}CD103^{-} DCs produced significantly higher levels of IL-23 (Figure 6A). To count T_H17 cells from the LP and MLNs, we subjected CD3^{+}CD4^{+} T cells to intracellular staining for IL-17 (Figure S6). The absolute number of T_H17 cells was significantly increased in the *CD137*$^{-/-}$ LP (Figure 6B), and so was their frequency in total T cells (Figures 6C and 6D). Increased percentages of T_H17 cells in the T cell population were also found in the LP and MLNs of *CD11c*^{Cre}*CD137*$^{fl/fl}$ mice (Figures 6E and 6F). In aggregate, the data presented so far indicate that RA may be a major effector for CD137 signaling to suppress CD11b^{+}CD103^{-} DCs in the inhibition of T_H17-mediated colitis. Indeed, administration of RA had a protective effect on colitis in *CD11c*^{Cre}*CD137*$^{fl/fl}$ mice (Figures 6G and 6H). RA administration also ameliorated colitis in *CD137*$^{fl/fl}$ mice, but its effect seemed to be less prominent compared to that in *CD11c*^{Cre}*CD137*$^{fl/fl}$ mice (Figures 6G and 6H). This protection was correlated with decreased percentages of IL-23^{+}CD11b^{+}CD103^{-} DCs and T_H17 cells in the LP and MLNs of *CD11c*^{Cre}*CD137*$^{fl/fl}$ mice (Figures 6I and 6J).

CD137 Stimulation Attenuates the Severity of Acute Colitis

As anti-CD137 agonistic antibodies are known to have therapeutic effects on colitis (Lee et al., 2005), we examined whether these effects arise from the stimulation of CD137 in CD11b^{-}CD103^{+} DCs. Multiple injections of anti-CD137 antibody starting from day −1 of DSS treatment were found to protect the host against DSS-induced colitis (Figures 7A–7E). This protection was associated with increased *Bcl-2* expression and RALDH2 activity in LP and MLN CD11b^{-}CD103^{+} DCs (Figures S7A–S7C) but not in CD11b^{+}CD103^{-} DCs (data not shown). Although the anti-CD137 antibody seemed to have a complex effect on the frequency of intestinal DC subsets (Figure S7D), its protective effect was not observed in *CD11c*^{Cre}*CD137*$^{fl/fl}$ mice (Figures 7F and 7G). As there was no difference in CD4^{+} T cell polarization between *CD11c*^{Cre}*CD137*$^{fl/fl}$ and *CD137*$^{fl/fl}$ mice, and anti-CD137 antibody did not affect this process in both groups (Figure S7E), DCs, but not CD4^{+} T cells, were likely to be necessary for its therapeutic effect on colitis.

DISCUSSION

Although immature DCs are well known to have a tolerogenic activity for immunity (Lutz and Schuler, 2002; Steinman and Nussenzweig, 2002), it is unclear how mature DCs control inflammation. In this study, using DC-specific *CD137*$^{-/-}$ mice, we identified CD137 as an immunosuppressive signal that regulates tolerogenic CD11b^{-}CD103^{+} DCs during acute intestinal inflammation. Our *in vitro* and *in vivo* results indicated that CD137 signaling is associated with three aspects of DC function: maturation, survival, and immunosuppression. These CD137-associated functions seem to be restricted mainly to intestinal CD11b^{-}CD103^{+} DCs. We do not know precisely why CD137 signaling is specific for this subset, but we can suggest several possible explanations. A unique intestinal microenvironment exposed to commensal microbiota and food antigens is likely to prime CD11b^{-}CD103^{+} to preferentially increase CD137 expression in response to inflammatory mediators. Once expressed, CD137 delivers signals that enforce immunosuppressive activities and mediate cell maturation and survival. In this case, homotypic cell-cell interactions seem to be sufficient to engage CD137 (Figure 4). Interestingly, a previous study showed that, within tumors, CD137L signaling is critical for the differentiation of immunosuppressive CD11b^{+}CD103^{-} DC2s, and its blockade promotes the differentiation of IL-12-producing CD103^{+} DC1s (Kang et al., 2017). In the intestine, however, our results demonstrated that CD137 signaling is required for the

Figure 3. DC-Specific CD137 Deficiency Exacerbates Acute Colitis

(A) Representative fluorescence-activated cell sorting (FACS) histograms for CD137 expression in LP DC subsets of noncolitic or colitic *CD137*$^{+/+}$ mice.

(B) Flow-cytometric analysis of CD137 expression in LP DC subsets of noncolitic (n = 4) or colitic *CD137*$^{+/+}$ mice (n = 4). Data are presented as mean ± SEM. ***p < 0.001 (Student's t test).

(C) Body weight changes of colitic *CD137*$^{fl/fl}$ (n = 9), *Lyz2*^{Cre}*CD137*$^{fl/fl}$ (n = 9), and *CD11c*^{Cre}*CD137*$^{fl/fl}$ (n = 9) mice. Data are presented as mean ± SEM. ***p < 0.001 (Student's t test).

(D) Colon length of colitic *CD137*$^{fl/fl}$ (n = 9), *Lyz2*^{Cre}*CD137*$^{fl/fl}$ (n = 9), and *CD11c*^{Cre}*CD137*$^{fl/fl}$ (n = 9) mice. **p < 0.01 (Student's t test).

(E) Representative microscopic images of H&E-stained colon sections of colitic *CD137*$^{fl/fl}$, *Lyz2*^{Cre}*CD137*$^{fl/fl}$, and *CD11c*^{Cre}*CD137*$^{fl/fl}$ mice. Scale bars, 100 μm.

(F) Crypt damage scores of colitic *CD137*$^{fl/fl}$ (n = 9), *Lyz2*^{Cre}*CD137*$^{fl/fl}$ (n = 12), and *CD11c*^{Cre}*CD137*$^{fl/fl}$ (n = 11) mice. ***p < 0.001 (Student's t test).

(G and H) Flow-cytometric analysis for LP (G) and MLN (H) DCs of *CD137*$^{fl/fl}$ (n = 8 in LP; n = 7 in MLN) and *CD11c*^{Cre}*CD137*$^{fl/fl}$ mice (n = 7 in LP; n = 9 in MLN). *p < 0.05; ***p < 0.001 (Student's t test).

See also Figure S4.

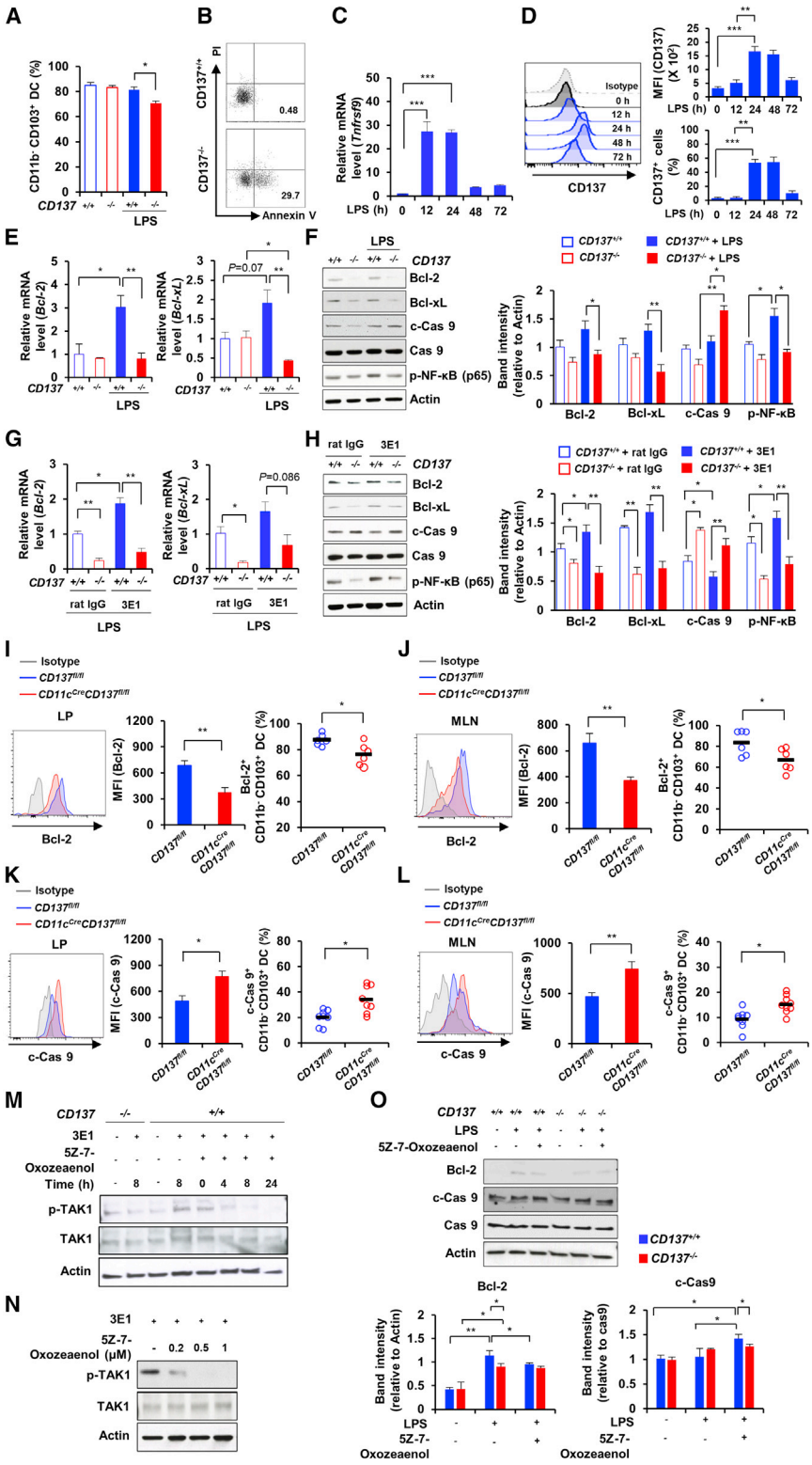

Figure 4. CD137 Deficiency Promotes Apoptosis of CD11b^{-}CD103^{+} DCs

(A) Portions of polarized CD11b^{-}CD103^{+} DCs in *CD137*$^{+/+}$ and *CD137*$^{-/-}$ BMDCs after stimulation with LPS for 24 h. Data are presented as mean ± SEM of three independent experiments. *p < 0.05 (Student's t test).

(B) Representative FACS dot plots for propium iodide (PI) and annexin V staining in polarized CD11b^{-}CD103^{+} DCs of *CD137*$^{+/+}$ (n = 4) and *CD137*$^{-/-}$ BMDCs (n = 4) after stimulation with LPS for 24 h.

(C and D) Analysis for expression of *Tnfrsf9* mRNA (C) and cell-surface CD137 protein (D) in *CD137*$^{+/+}$ CD11b^{-}CD103^{+} BMDCs after stimulation with LPS for the indicated time. *Tnfrsf9* expression was normalized to *Actb* expression. Data are presented as mean ± SEM of three independent experiments. **p < 0.01; ***p < 0.001 (one-way ANOVA with Bonferroni correction).

(E) Real-time PCR analysis for expression of *Bcl-2* and *Bcl-xL* in *CD137*$^{+/+}$ and *CD137*$^{-/-}$ CD11b^{-}CD103^{+} BMDCs after stimulation with LPS for 12 h. Data were normalized to *Actb* expression and are presented as mean ± SEM of three independent experiments. *p < 0.05; **p < 0.01 (Student's t test).

(F) Western blot analysis for Bcl-2, Bcl-xL, caspase-9 (Cas 9), cleaved caspase-9 (c-Cas 9), and phosphorylated NF-κB (p-NF-κB) in *CD137*$^{+/+}$ and *CD137*$^{-/-}$ CD11b^{-}CD103^{+} BMDCs in response to LPS for 24 h. Data were normalized to actin band intensities and are presented as mean ± SEM of three independent experiments. *p < 0.05; **p < 0.01 (Student's t test).

(G) Real-time PCR analysis for expression of *Bcl-2* and *Bcl-xL* in *CD137*$^{+/+}$ and *CD137*$^{-/-}$ CD11b^{-}CD103^{+} BMDCs in response to rat IgG or anti-CD137 antibody (3E1). Data were normalized to *Actb* expression and are presented as mean ± SEM of three independent experiments. *p < 0.05; **p < 0.01 (Student's t test).

(H) Western blot analysis for Bcl-2, Bcl-xL, Cas 9, c-Cas 9, and p-NF-κB in *CD137*$^{+/+}$ and *CD137*$^{-/-}$ CD11b^{-}CD103^{+} BMDCs in response to rat IgG or 3E1 for 24 h. Data were normalized to actin band intensities and are presented as mean ± SEM of three independent experiments. *p < 0.05; **p < 0.01 (Student's t test).

(I and J) Flow-cytometric analysis for intracellular Bcl-2 in LP (I) and MLN (J) CD11b^{-}CD103^{+} DCs of colitic *CD137*$^{fl/fl}$ (n = 6) and *CD11c*^{Cre}*CD137*$^{fl/fl}$ (n = 6) mice. Data are presented as mean ± SEM. *p < 0.05 (Student's t test).

(K and L) Flow-cytometric analysis for intracellular Bcl-2 expression in LP (K) and MLN (L) CD11b^{-}CD103^{+} DCs of colitic *CD137*$^{fl/fl}$ (n = 8) and *CD11c*^{Cre}*CD137*$^{fl/fl}$ (n = 8) mice. Data are presented as mean ± SEM. *p < 0.05; **p < 0.01 (Student's t test).

(M) Western blot analysis for TAK1 and p-TAK1 in *CD137*$^{+/+}$ and *CD137*$^{-/-}$ CD11b^{-}CD103^{+} BMDCs in response to 3E1 in the presence of 5Z-7-oxozeaenol (TAK1 inhibitor; 0.5 μM; 2-h pretreatment) for 8 h.

(legend continued on next page)

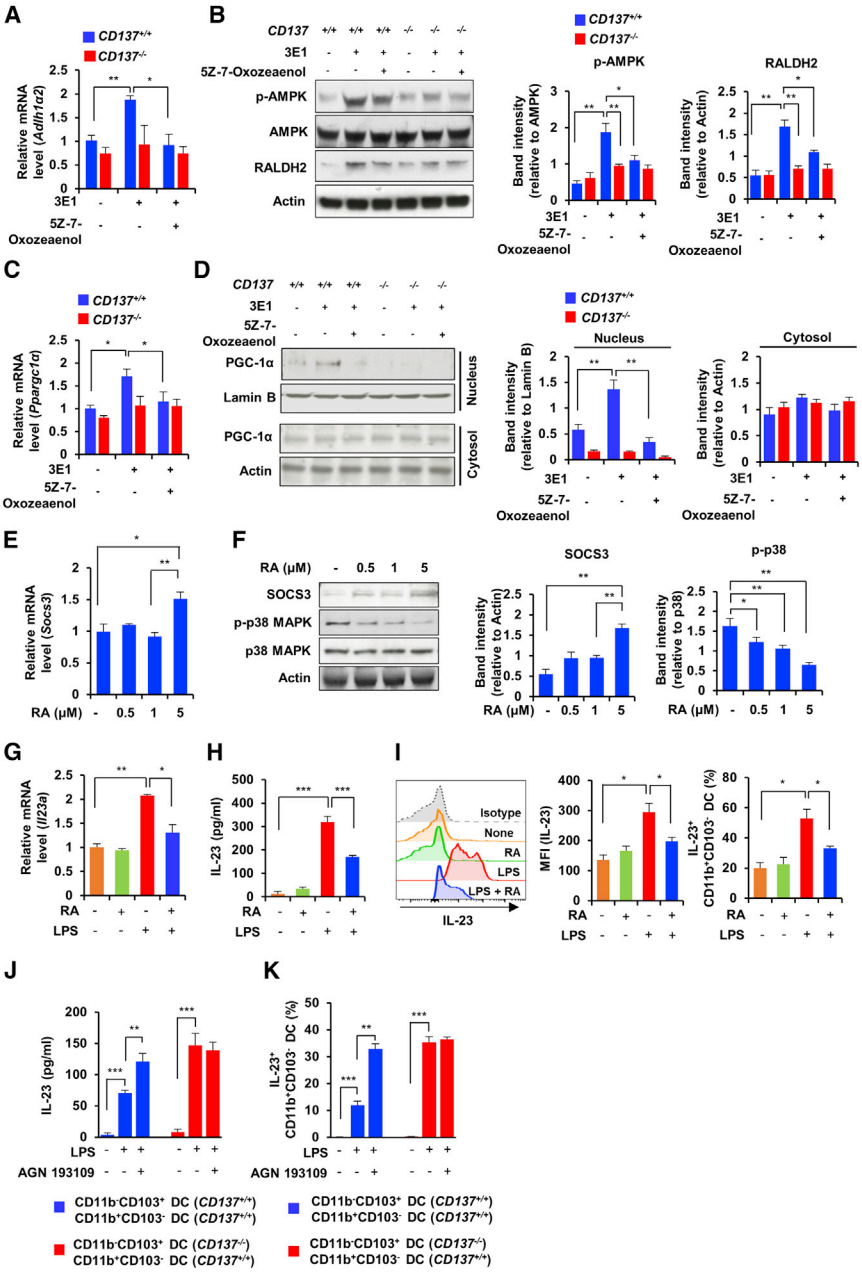

Figure 5. CD137 Signaling Promotes RA Production via the TAK1-AMPK-PGC1α Axis

(A) Real-time PCR analysis for expression of *Adlh1a2* in *CD137*$^{+/+}$ and *CD137*$^{-/-}$ CD11b^{-}CD103^{+} BMDCs in response to 3E1 in the presence of 5Z-7-oxozeaenol (0.5 μM; 2-h pretreatment) for 12 h. Data were normalized to *Actb* expression and are presented as mean ± SEM of three independent experiments. *p < 0.05; **p < 0.01 (Student's t test).

(B) Western blot analysis for AMPK, phosphoylated (p)-AMPK, and RALDH2 in *CD137*$^{+/+}$ and *CD137*$^{-/-}$ CD11b^{-}CD103^{+} BMDCs in response to 3E1 in the presence of 5Z-7-oxozeaenol (0.5 μM; 2-h pretreatment) for 24 h. Data were normalized to actin band intensities and are presented as mean ± SEM of three independent experiments. *p < 0.05; **p < 0.01 (Student's t test).

(C) Real-time PCR analysis for expression of *Ppargc1a* in *CD137*$^{+/+}$ and *CD137*$^{-/-}$ CD11b^{-}CD103^{+} BMDCs in response to 3E1 in the presence of 5Z-7-oxozeaenol (0.5 μM; 2-h pretreatment) for 12 h. Data were normalized to *Actb* expression and are presented as mean ± SEM of three independent experiments. *p < 0.05 (Student's t test).

(D) Western blot analysis for nuclear and cytosolic PGC-1α in *CD137*$^{+/+}$ and *CD137*$^{-/-}$ CD11b^{-}CD103^{+} BMDCs in response to 3E1 in the presence of 5Z-7-oxozeaenol (0.5 μM; 2-h pretreatment) for 24 h. Data were normalized to lamin B or actin band intensities and are presented as mean ± SEM of three independent experiments. *p < 0.05; **p < 0.01 (Student's t test).

(E) Real-time PCR analysis for expression of *Socs3* in *CD137*$^{+/+}$ CD11b^{+}CD103^{-} BMDCs in response to RA for 12 h. Data were normalized to *Actb* expression and are presented as mean ± SEM of three independent experiments. *p < 0.05; **p < 0.01 (01 (one-way ANOVA with Bonferroni correction).

(F) Western blot analysis for SOCS3, p38MAPK, and p-p38MAPK in *CD137*$^{+/+}$ CD11b^{+}CD103^{-} BMDCs in response to RA for 24 h. Data were normalized to actin or p38MAPK band intensities and are presented as mean ± SEM of three independent experiments. *p < 0.05; **p < 0.01 (one-way ANOVA test with Bonferroni correction).

(G–I) Analysis for *Il23a* mRNA (G) and secreted (H) or intracellular (I) IL-23 protein of *CD137*$^{+/+}$ CD11b^{+}CD103^{-} BMDCs in response to LPS in the presence of RA for 12 h (G) or 24 h (H and I). Data are presented as mean ± SEM of three independent experiments. *p < 0.05; **p < 0.01; ***p < 0.001 (Student's t test).

(J and K) Analysis for secreted (J) or intracellular IL-23 (K) of *CD137*$^{+/+}$ CD11b^{+}CD103^{-} BMDCs cocultured with *CD137*$^{+/+}$ or *CD137*$^{-/-}$ CD11b^{-}CD103^{+} BMDCs in response to LPS in the presence of RAR antagonist (AGN 193109). Data are presented as mean ± SEM of three independent experiments. **p < 0.01; ***p < 0.001 (Student's t test).

CD11b^{-}CD103^{+} subset to suppress the activity of the pathogenic IL-23-producing CD11b^{+}CD103^{-} subset during colitis. Our *in vitro* results indicate that interactions between CD137 and CD137L on LPS-activated CD11b^{-}CD103^{+} DCs should be critical in triggering CD137 signaling (Figure S4D) (Mbanwi et al., 2017). However, *CD137L*$^{-/-}$ and WT mice did not exhibit any difference in disease

(N) Western blot analysis for TAK1 and p-TAK1 in *CD137*$^{+/+}$ and *CD137*$^{-/-}$ CD11b^{-}CD103^{+} BMDCs in response to 3E1 in the presence of various doses of 5Z-7-oxozeaenol for 8 h.

(O) Western blot analysis for Bcl-2, Cas 9, and c-Cas 9 in *CD137*$^{+/+}$ and *CD137*$^{-/-}$ CD11b^{-}CD103^{+} BMDCs in the presence of 5Z-7-oxozeaenol (0.5 μM; 2-h pretreatment) for 24 h. Data were normalized to actin band intensities and are presented as mean ± SEM of three independent experiments. *p < 0.05; **p < 0.01 (Student's t test).

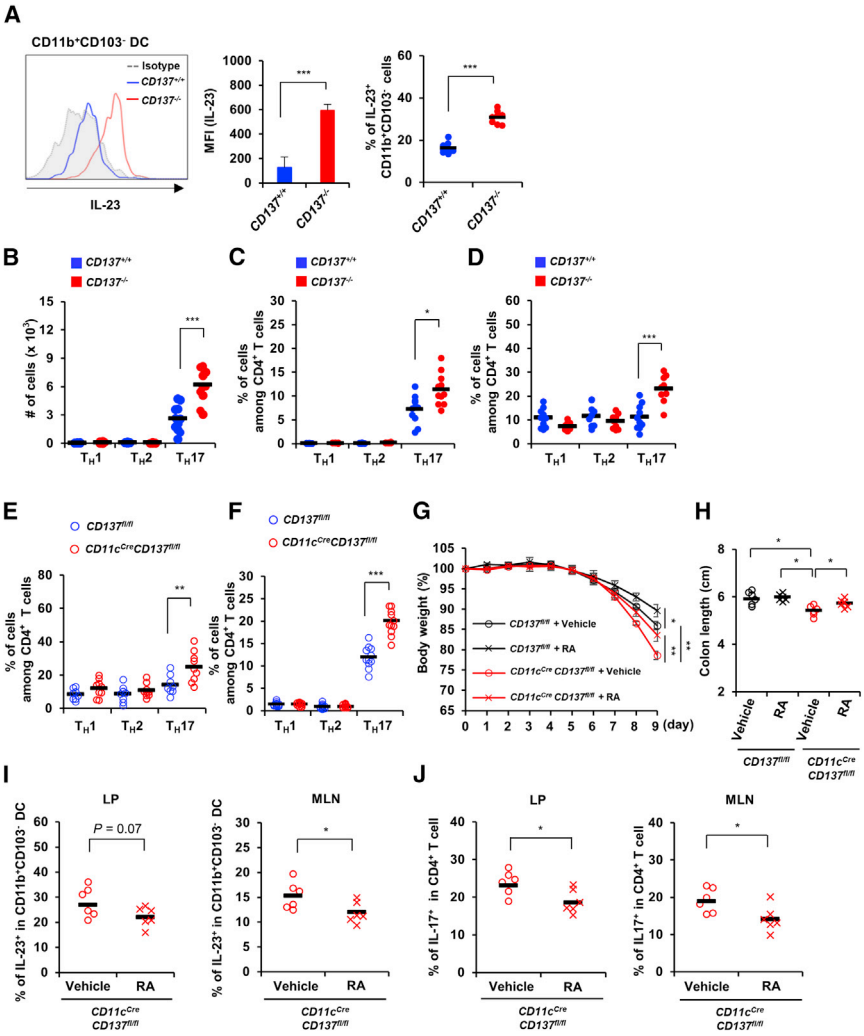

Figure 6. *CD137* Deficiency Promotes the Differentiation of T_H17 Cells

(A) Flow-cytometric analysis for intracellular IL-23 in LP $CD11b^+CD103^-$ DCs of colitic $CD137^{+/+}$ (n = 8) and $CD137^{-/-}$ mice (n = 8). Data are presented as mean ± SEM. ***p < 0.001 (Student's t test).

(B–D) Flow-cytometric analysis for numbers (B) and percentages (C) of LP T_H subsets in colitic $CD137^{+/+}$ (n = 11) and $CD137^{-/-}$ (n = 11) mice and MLN T_H subsets (D) of colitic $CD137^{+/+}$ (n = 10) and $CD137^{-/-}$ (n = 9) mice. *p < 0.05; ***p < 0.001 (Student's t test).

(E and F) Flow-cytometric analysis for LP (E) and MLN (F) T_H subsets of colitic $CD137^{fl/fl}$ (n = 8 in LP; n = 11 in MLN) and $CD11c^{cre}CD137^{fl/fl}$ (n = 9 in LP; n = 11 in MLN) mice. **p < 0.01; ***p < 0.001 (Student's t test).

(G) Body weight changes of RA- or vehicle-injected colitic $CD137^{fl/fl}$ (n = 6 each group), and $CD11c^{Cre}CD137^{fl/fl}$ (n = 6 each group) mice. ***p < 0.05 (Student's t test).

(H) Colon length of RA- or vehicle-injected colitic $CD137^{fl/fl}$ (n = 6 each group) and $CD11c^{Cre}CD137^{fl/fl}$ (n = 6 each group) mice. *p < 0.05; *p < 0.01 (Student's t test).

(I) Flow-cytometric analysis of intracellular IL-23 production by LP and MLN $CD11b^+CD103^-$ DCs of colitic $CD11c^{Cre}CD137^{fl/fl}$ mice injected with vehicle (n = 6 each group) or RA (n = 6 each group). *p < 0.05 (Student's t test).

(J) Flow-cytometric analysis for LP and MLN T_H17 cells of $CD11c^{Cre}CD137^{fl/fl}$ mice injected with vehicle (n = 6 each group) or RA (n = 6 each group). *p < 0.05 (Student's t test).

See also Figure S6.

severity in our colitis model (Figure S1), suggesting that there may exist an as-yet-unidentified CD137L. Signaling through a CD137L of this nature has been implicated in the induction of tumor growth-associated DC2 and M2 macrophage differentiation within tumors (Kang et al., 2017; Kwon, 2018). As *CD137L*$^{-/-}$ mice have increased IL-4-dependent immunoglobulin G_1 (IgG_1) antibody responses (unpublished data), it seems that there is a competition between these two CD137 ligands for binding to CD137. It is also noteworthy that immune dysregulation is observed only in *CD137*$^{-/-}$ mice, probably because of the absence of regulatory CD137 signaling. This hypothesis is currently under investigation in our laboratory.

The earliest signaling event after the engagement of CD137 is the recruitment of TRAF1 and TRAF2 to the intracellular domain of CD137, which is thought to be followed by the polyubiquitination of TRAF2 (Martinez-Forero et al., 2013). Our results showed that TAK1, which is a substrate for TRAF2 ubiquitin ligase (Ea et al., 2006), is phosphorylated in $CD11b^-CD103^+$ DCs after the engagement of CD137 and that it regulates the survival of these cells via the upregulation of the NF-κB target genes *Bcl-2* and *Bcl-xL* and the decreased cleavage of caspase-9 (Figure 4). TAK1 was also found to be critical in regulating the immunosuppressive activity of these cells through activation of AMPK and its downstream signaling partner, PCG-1α. This signaling axis is indispensable for the expression of RA, which, in turn, increases SOCS3 expression in adjacent $CD11b^+CD103^-$ DCs to suppress p38MAPK, which is required for IL-23 production (Figure 5). Given the critical role of IL-23 in pathogenic T_H17 cell differentiation (Kobayashi et al., 2008; Kara et al., 2015), we propose that the RA-mediated inhibition of $CD11b^+CD103^-$ DC activity may be an important stage of immune regulation in the intestine. However, RA is likely to have a broad range of immunosuppressive activities against a variety of immune cells, either directly or via Treg cells (Larange and Cheroutre, 2016). It is also generally accepted that RA and other immunosuppressive mediators (e.g., kynurenines, IL-10, and IL-27) cross-regulate each other in autocrine and paracrine manners (Quintana et al., 2010).

Agonistic anti-CD137 antibodies have potent therapeutic effects on various autoimmune and inflammatory diseases (Seo et al., 2004; Lee and Croft, 2009). Accumulating evidence suggests that anti-CD137-mediated immunosuppression is operated by two distinguishable mechanisms: deletion of T_{eff} cells through activation of cell death pathways, including the Fas pathway (Kim et al., 2005; Asai et al., 2007; Zhang and Mittler, 2007) and anergy of pathogenic T cells (Foell et al., 2003).

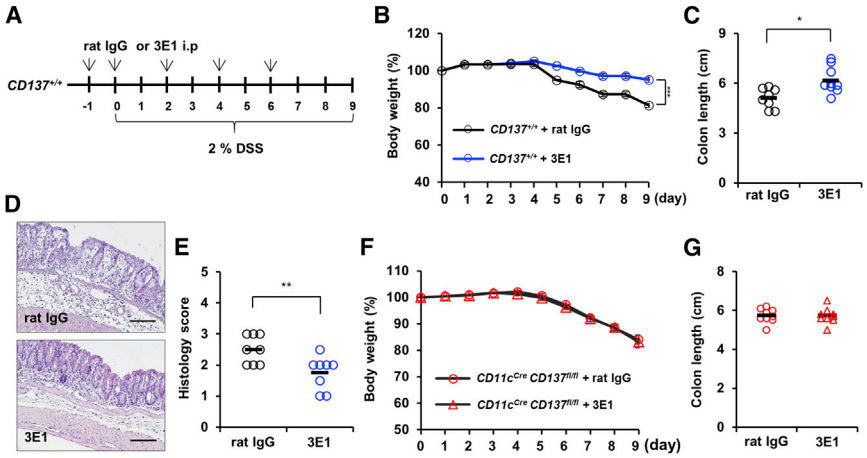

Figure 7. Activation of CD137 Signaling Inhibits Acute Colitis

(A) An experimental scheme.

(B) Body weight changes of colitic *CD137*$^{+/+}$ mice injected with 3E1 (n = 9) or control IgG (n = 8). Data are presented as mean ± SEM. ***p < 0.001 (Student's t test).

(C) Colon length of colitic *CD137*$^{+/+}$ mice injected with 3E1 (n = 9) or rat IgG (n = 8). *p < 0.05 (Student's t test).

(D) Representative images of H&E-stained colon sections of 3E1- or rat IgG-injected colitic *CD137*$^{+/+}$ mice. Scale abrs, 100 μm.

(E) Scores for colonic tissue disruption of 3E1- or rat IgG-injected colitic *CD137*$^{+/+}$ mice (n = 8). **p < 0.01 (Student's t test).

(F) Body weight changes of colitic *CD11c*^{Cre}*CD137*$^{fl/fl}$ mice injected with 3E1 (n = 8) or rat IgG (n = 8).

(G) Colon length of colitic *CD11c*^{Cre}*CD137*$^{fl/fl}$ mice injected with 3E1 (n = 8) or rat IgG (n = 8).

See also Figure S7.

The interface of DCs and T cells is important for these two mechanisms (Foell et al., 2003; Zhang et al., 2010). Immunosuppressive or tolerogenic DCs generated by CD137 signaling seem to be heterogeneous; here, we propose that they can be broadly classified into two groups, even though their phenotypes and functions can overlap. In the first category of DCs, CD137 signaling contributes to the production of immunosuppressive effector molecules, including kynurenines, RA, and cytokines (e.g., IL-10 and IL-27). Intestinal CD11b^{-}CD103^{+} DCs are representative of this category, but phenotypic diversity exists among these cells in organs other than the intestine (Iberg et al., 2017). The second category of DCs may be phenotypically heterogeneous, but they commonly induce the cell death of T_{eff} cells via stimulation of death receptors. Thus, these DCs are likely to express molecules related to cell death and exhaustion (e.g., FasL, tumor necrosis factor alpha [TNF-α], PD-L1, PD-L2, perforins, and granzymes) (Yogev et al., 2012; Zlotnikov-Klionsky et al., 2015). In sum, our results and those of other groups suggest that CD137 signaling induces different subsets of tolerogenic DCs, depending on the context of the immune response(s) (Zhang and Mittler, 2007; Zhang et al., 2010; Lee et al., 2012).

Previously, it was not known why *CD137*$^{-/-}$ mice exhibit dysregulated immune responses in some experimental settings (Kwon et al., 2002). Our results may provide important insights into this impaired immune regulation in *CD137*$^{-/-}$ mice. We believe that a large part of the immunosuppressive activities driven by the engagement of CD137 (either by its natural ligand or by an anti-CD137 antibody) is mediated by tolerogenic DCs and that a microenvironment in which an immune response occurs seems to be critical in determining whether stimulatory DCs or tolerogenic DCs are co-opted. Together, our results indicate that the CD137-CD137L system is an important component of the immunosuppressive intestinal microenvironment.

STAR★METHODS

Detailed methods are provided in the online version of this paper and include the following:

SUPPLEMENTAL INFORMATION

Supplemental Information can be found online at https://doi.org/10.1016/j.celrep.2020.02.103.

ACKNOWLEDGMENTS

This work was supported by National Research Foundation of Korea (NRF) grants funded by the Korean government (NRF-2012R1A3A2026454, NRF-2015M3A9B6029138, and NRF-2017R1A2B3008475).

AUTHOR CONTRIBUTIONS

J.J., B.K., and G.T.O. designed the experiments, interpreted data, and wrote the manuscript. J.J. performed most of the experiments, with help from I.-H.J., S.H.M., S.J., S.-J.J., S.-K.S., S.S., M.-N.L., E.J.S., H.Y.K., S.K., T.K.K., and J.K. H.R.C. and J.-H.C. gave critical comments. All authors actively discussed and reviewed the manuscript.

DECLARATION OF INTERESTS

The authors declare no competing interests.

Received: September 22, 2019
Revised: December 21, 2019
Accepted: February 27, 2020
Published: March 24, 2020

REFERENCES

Abe, K., Nguyen, K.P., Fine, S.D., Mo, J.H., Shen, C., Shenouda, S., Corr, M., Jung, S., Lee, J., Eckmann, L., and Raz, E. (2007). Conventional dendritic cells regulate the outcome of colonic inflammation independently of T cells. Proc. Natl. Acad. Sci. USA *104*, 17022–17027.

Asai, T., Choi, B.K., Kwon, P.M., Kim, W.Y., Kim, J.D., Vinay, D.S., Gebhardt, B.M., and Kwon, B.S. (2007). Blockade of the 4-1BB (CD137)/4-1BBL and/or CD28/CD80/CD86 costimulatory pathways promotes corneal allograft survival in mice. Immunology *121*, 349–358.

Berndt, B.E., Zhang, M., Chen, G.H., Huffnagle, G.B., and Kao, J.Y. (2007). The role of dendritic cells in the development of acute dextran sulfate sodium colitis. J. Immunol. *179*, 6255–6262.

Bogunovic, M., Ginhoux, F., Helft, J., Shang, L., Hashimoto, D., Greter, M., Liu, K., Jakubzick, C., Ingersoll, M.A., Leboeuf, M., et al. (2009). Origin of the lamina propria dendritic cell network. Immunity *31*, 513–525.

Broadhurst, M.J., Leung, J.M., Lim, K.C., Girgis, N.M., Gundra, U.M., Fallon, P.G., Premenko-Lanier, M., McKerrow, J.H., McCune, J.M., and Loke, P. (2012). Upregulation of retinal dehydrogenase 2 in alternatively activated macrophages during retinoid-dependent type-2 immunity to helminth infection in mice. PLoS Pathog. *8*, e1002883.

Choi, B.K., Kim, Y.H., Kwon, P.M., Lee, S.C., Kang, S.W., Kim, M.S., Lee, M.J., and Kwon, B.S. (2009). 4-1BB functions as a survival factor in dendritic cells. J. Immunol. *182*, 4107–4115.

Dasgupta, S., Erturk-Hasdemir, D., Ochoa-Reparaz, J., Reinecker, H.C., and Kasper, D.L. (2014). Plasmacytoid dendritic cells mediate anti-inflammatory responses to a gut commensal molecule via both innate and adaptive mechanisms. Cell Host Microbe *15*, 413–423.

DeBenedette, M.A., Wen, T., Bachmann, M.F., Ohashi, P.S., Barber, B.H., Stocking, K.L., Peschon, J.J., and Watts, T.H. (1999). Analysis of 4-1BB ligand (4-1BBL)-deficient mice and of mice lacking both 4-1BBL and CD28 reveals a role for 4-1BBL in skin allograft rejection and in the cytotoxic T cell response to influenza virus. J. Immunol. *163*, 4833–4841.

Durai, V., and Murphy, K.M. (2016). Functions of murine dendritic cells. Immunity *45*, 719–736.

Ea, C.K., Deng, L., Xia, Z.P., Pineda, G., and Chen, Z.J.J. (2006). Activation of IKK by TNFalpha requires site-specific ubiquitination of RIP1 and polyubiquitin binding by NEMO. Mol. Cell *22*, 245–257.

Eichele, D.D., and Kharbanda, K.K. (2017). Dextran sodium sulfate colitis murine model: an indispensable tool for advancing our understanding of inflammatory bowel diseases pathogenesis. World J. Gastroenterol. *23*, 6016–6029.

Eun, S.Y., Lee, S.W., Xu, Y., and Croft, M. (2015). 4-1BB ligand signaling to T cells limits T cell activation. J. Immunol. *194*, 134–141.

Foell, J., McCausland, M., Burch, J., Corriazzi, N., Yan, X.J., Suwyn, C., O'Neil, S.P., Hoffmann, M.K., and Mittler, R.S. (2003). CD137-mediated T cell co-stimulation terminates existing autoimmune disease in SLE-prone NZB/NZW F1 mice. Ann. N Y Acad. Sci. *987*, 230–235.

Grajales-Reyes, G.E., Iwata, A., Albring, J., Wu, X., Tussiwand, R., Kc, W., Kretzer, N.M., Briseño, C.G., Durai, V., Bagadia, P., et al. (2015). Batf3 maintains autoactivation of Irf8 for commitment of a CD8α(+) conventional DC clonogenic progenitor. Nat. Immunol. *16*, 708–717.

Guilliams, M., Ginhoux, F., Jakubzick, C., Naik, S.H., Onai, N., Schraml, B.U., Segura, E., Tussiwand, R., and Yona, S. (2014). Dendritic cells, monocytes and macrophages: a unified nomenclature based on ontogeny. Nat. Rev. Immunol. *14*, 571–578.

Hsieh, E.H., Fernandez, X., Wang, J., Hamer, M., Calvillo, S., Croft, M., Kwon, B.S., and Lo, D.D. (2010). CD137 is required for M cell functional maturation but not lineage commitment. Am. J. Pathol. *177*, 666–676.

Huang, Y.L., Chassard, C., Hausmann, M., von Itzstein, M., and Hennet, T. (2015). Sialic acid catabolism drives intestinal inflammation and microbial dysbiosis in mice. Nat. Commun. *6*, 8141.

Iberg, C.A., Jones, A., and Hawiger, D. (2017). Dendritic cells as inducers of peripheral tolerance. Trends Immunol. *38*, 793–804.

Izcue, A., Coombes, J.L., and Powrie, F. (2006). Regulatory T cells suppress systemic and mucosal immune activation to control intestinal inflammation. Immunol. Rev. *212*, 256–271.

Jäger, S., Handschin, C., St-Pierre, J., and Spiegelman, B.M. (2007). AMP-activated protein kinase (AMPK) action in skeletal muscle via direct phosphorylation of PGC-1alpha. Proc. Natl. Acad. Sci. USA *104*, 12017–12022.

Jang, M.H., Sougawa, N., Tanaka, T., Hirata, T., Hiroi, T., Tohya, K., Guo, Z., Umemoto, E., Ebisuno, Y., Yang, B.G., et al. (2006). CCR7 is critically important in intestinal lamina propria for migration of dendritic cells to mesenteric lymph nodes. J. Immunol. *176*, 803–810.

Jeon, H.J., Choi, J.H., Jung, I.H., Park, J.G., Lee, M.R., Lee, M.N., Kim, B., Yoo, J.Y., Jeong, S.J., Kim, D.Y., et al. (2010). CD137 (4-1BB) deficiency reduces atherosclerosis in hyperlipidemic mice. Circulation *121*, 1124–1133.

Joeris, T., Müller-Luda, K., Agace, W.W., and Mowat, A.M. (2017). Diversity and functions of intestinal mononuclear phagocytes. Mucosal Immunol. *10*, 845–864.

Kang, S.W., Lee, S.C., Park, S.H., Kim, J., Kim, H.H., Lee, H.W., Seo, S.K., Kwon, B.S., Cho, H.R., and Kwon, B. (2017). Anti-CD137 suppresses tumor growth by blocking reverse signaling by CD137 ligand. Cancer Res. *77*, 5989–6000.

Kara, E.E., McKenzie, D.R., Bastow, C.R., Gregor, C.E., Fenix, K.A., Ogunniyi, A.D., Paton, J.C., Mack, M., Pombal, D.R., Seillet, C., et al. (2015). CCR2 defines in vivo development and homing of IL-23-driven GM-CSF-producing Th17 cells. Nat. Commun. *6*, 8644.

Kiesler, P., Fuss, I.J., and Strober, W. (2015). Experimental models of inflammatory bowel diseases. Cell. Mol. Gastroenterol. Hepatol. *1*, 154–170.

Kim, J., Choi, W.S., La, S., Suh, J.H., Kim, B.S., Cho, H.R., Kwon, B.S., and Kwon, B. (2005). Stimulation with 4-1BB (CD137) inhibits chronic graft-versus-host disease by inducing activation-induced cell death of donor CD4+ T cells. Blood *105*, 2206–2213.

Kim, H.J., Lee, J.S., Kim, J.D., Cha, H.J., Kim, A., Lee, S.K., Lee, S.C., Kwon, B.S., Mittler, R.S., Cho, H.R., and Kwon, B. (2012). Reverse signaling through the costimulatory ligand CD137L in epithelial cells is essential for natural killer cell-mediated acute tissue inflammation. Proc. Natl. Acad. Sci. U S A *109*, E13–E22.

Kobayashi, T., Okamoto, S., Hisamatsu, T., Kamada, N., Chinen, H., Saito, R., Kitazume, M.T., Nakazawa, A., Sugita, A., Koganei, K., et al. (2008). IL23 differentially regulates the Th1/Th17 balance in ulcerative colitis and Crohn's disease. Gut *57*, 1682–1689.

Kwon, B. (2012). Regulation of inflammation by bidirectional signaling through CD137 and its ligand. Immune Netw. *12*, 176–180.

Kwon, B. (2018). Anti-CD137 cancer immunotherapy suppresses tumor growth-response. Cancer Res. *78*, 1572–1573.

Kwon, B.S., Hurtado, J.C., Lee, Z.H., Kwack, K.B., Seo, S.K., Choi, B.K., Koller, B.H., Wolisi, G., Broxmeyer, H.E., and Vinay, D.S. (2002). Immune responses in 4-1BB (CD137)-deficient mice. J. Immunol. *168*, 5483–5490.

Langstein, J., Michel, J., Fritsche, J., Kreutz, M., Andreesen, R., and Schwarz, H. (1998). CD137 (ILA/4-1BB), a member of the TNF receptor family, induces monocyte activation via bidirectional signaling. J. Immunol. *160*, 2488–2494.

Larange, A., and Cheroutre, H. (2016). Retinoic acid and retinoic acid receptors as pleiotropic modulators of the immune system. Annu. Rev. Immunol. *34*, 369–394.

Lee, S.W., and Croft, M. (2009). 4-1BB as a therapeutic target for human disease. Adv. Exp. Med. Biol. *647*, 120–129.

Lee, S.W., Park, Y., So, T., Kwon, B.S., Cheroutre, H., Mittler, R.S., and Croft, M. (2008). Identification of regulatory functions for 4-1BB and 4-1BBL in myelopoiesis and the development of dendritic cells. Nat. Immunol. *9*, 917–926.

Lee, J., Kim, E.N., Park, H.J., Chang, C.Y., Jung, D.Y., Choi, C.Y., Lee, S.K., Kwon, G.Y., Joh, J.W., Kim, S.J., et al. (2005). Administration of agonistic anti-4-1BB monoclonal antibody leads to the amelioration of inflammatory bowel disease. Immunol. Lett. *101*, 210–216.

Lee, S.W., Park, Y., Eun, S.Y., Madireddi, S., Cheroutre, H., and Croft, M. (2012). Cutting edge: 4-1BB controls regulatory activity in dendritic cells through promoting optimal expression of retinal dehydrogenase. J. Immunol. *189*, 2697–2701.

Lin, J., Handschin, C., and Spiegelman, B.M. (2005). Metabolic control through the PGC-1 family of transcription coactivators. Cell Metab. *1*, 361–370.

Lutz, M.B., and Schuler, G. (2002). Immature, semi-mature and fully mature dendritic cells: which signals induce tolerance or immunity? Trends Immunol. *23*, 445–449.

Magnusson, M.K., Brynjólfsson, S.F., Dige, A., Uronen-Hansson, H., Börjesson, L.G., Bengtsson, J.L., Gudjonsson, S., Öhman, L., Agnholt, J., Sjövall, H., et al. (2016). Macrophage and dendritic cell subsets in IBD: ALDH+ cells are reduced in colon tissue of patients with ulcerative colitis regardless of inflammation. Mucosal Immunol. *9*, 171–182.

Mak, A., Dharmadhikari, B., Kow, N.Y., Thamboo, T.P., Tang, Q., Wong, L.W., Sajikumar, S., Wong, H.Y., and Schwarz, H. (2019). Deletion of CD137 ligand exacerbates renal and cutaneous but alleviates cerebral manifestations in lupus. Front. Immunol. *10*, 1411.

Manicassamy, S., and Pulendran, B. (2009). Retinoic acid-dependent regulation of immune responses by dendritic cells and macrophages. Semin. Immunol. *21*, 22–27.

Manicassamy, S., Ravindran, R., Deng, J., Oluoch, H., Denning, T.L., Kasturi, S.P., Rosenthal, K.M., Evavold, B.D., and Pulendran, B. (2009). Toll-like receptor 2-dependent induction of vitamin A-metabolizing enzymes in dendritic cells promotes T regulatory responses and inhibits autoimmunity. Nat. Med. *15*, 401–409.

Martinez-Forero, I., Azpilikueta, A., Bolaños-Mateo, E., Nistal-Villan, E., Palazon, A., Teijeira, A., Perez-Chacon, G., Morales-Kastresana, A., Murillo, O., Jure-Kunkel, M., et al. (2013). T cell costimulation with anti-CD137 monoclonal antibodies is mediated by K63-polyubiquitin-dependent signals from endosomes. J. Immunol. *190*, 6694–6706.

Martínez Gómez, J.M., Chen, L., Schwarz, H., and Karrasch, T. (2013). CD137 facilitates the resolution of acute DSS-induced colonic inflammation in mice. PLoS ONE *8*, e73277.

Mbanwi, A.N., Lin, G.H.Y., Wang, K.C., and Watts, T.H. (2017). Constitutive interaction between 4-1BB and 4-1BBL on murine LPS-activated bone marrow dendritic cells masks detection of 4-1BBL by TKS-1 but not 19H3 antibody. J. Immunol. Methods *450*, 81–89.

Melero, I., Shuford, W.W., Newby, S.A., Aruffo, A., Ledbetter, J.A., Hellström, K.E., Mittler, R.S., and Chen, L. (1997). Monoclonal antibodies against the 4-1BB T-cell activation molecule eradicate established tumors. Nat. Med. *3*, 682–685.

Nishimoto, H., Lee, S.W., Hong, H., Potter, K.G., Maeda-Yamamoto, M., Kinoshita, T., Kawakami, Y., Mittler, R.S., Kwon, B.S., Ware, C.F., et al. (2005). Costimulation of mast cells by 4-1BB, a member of the tumor necrosis factor receptor superfamily, with the high-affinity IgE receptor. Blood *106*, 4241–4248.

Quintana, F.J., Murugaiyan, G., Farez, M.F., Mitsdoerffer, M., Tukpah, A.M., Burns, E.J., and Weiner, H.L. (2010). An endogenous aryl hydrocarbon receptor ligand acts on dendritic cells and T cells to suppress experimental autoimmune encephalomyelitis. Proc. Natl. Acad. Sci. USA *107*, 20768–20773.

Satpathy, A.T., Briseño, C.G., Lee, J.S., Ng, D., Manieri, N.A., Kc, W., Wu, X., Thomas, S.R., Lee, W.L., Turkoz, M., et al. (2013). Notch2-dependent classical dendritic cells orchestrate intestinal immunity to attaching-and-effacing bacterial pathogens. Nat. Immunol. *14*, 937–948.

Schlitzer, A., McGovern, N., Teo, P., Zelante, T., Atarashi, K., Low, D., Ho, A.W.S., See, P., Shin, A., Wasan, P.S., et al. (2013). IRF4 transcription factor-dependent CD11b+ dendritic cells in human and mouse control mucosal IL-17 cytokine responses. Immunity *38*, 970–983.

Schlitzer, A., Sivakamasundari, V., Chen, J., Sumatoh, H.R., Schreuder, J., Lum, J., Malleret, B., Zhang, S., Larbi, A., Zolezzi, F., et al. (2015). Identification of cDC1- and cDC2-committed DC progenitors reveals early lineage priming at the common DC progenitor stage in the bone marrow. Nat. Immunol. *16*, 718–728.

Schwarz, H. (2005). Biological activities of reverse signal transduction through CD137 ligand. J. Leukoc. Biol. *77*, 281–286.

Scott, C.L., Bain, C.C., Wright, P.B., Sichien, D., Kotarsky, K., Persson, E.K., Luda, K., Guilliams, M., Lambrecht, B.N., Agace, W.W., et al. (2015). CCR2(+)CD103(-) intestinal dendritic cells develop from DC-committed precursors and induce interleukin-17 production by T cells. Mucosal Immunol. *8*, 327–339.

Seo, S.K., Choi, J.H., Kim, Y.H., Kang, W.J., Park, H.Y., Suh, J.H., Choi, B.K., Vinay, D.S., and Kwon, B.S. (2004). 4-1BB-mediated immunotherapy of rheumatoid arthritis. Nat. Med. *10*, 1088–1094.

Shuford, W.W., Klussman, K., Tritchler, D.D., Loo, D.T., Chalupny, J., Siadak, A.W., Brown, T.J., Emswiler, J., Raecho, H., Larsen, C.P., et al. (1997). 4-1BB costimulatory signals preferentially induce CD8+ T cell proliferation and lead to the amplification in vivo of cytotoxic T cell responses. J. Exp. Med. *186*, 47–55.

Steinman, R.M., and Nussenzweig, M.C. (2002). Avoiding horror autotoxicus: the importance of dendritic cells in peripheral T cell tolerance. Proc. Natl. Acad. Sci. USA *99*, 351–358.

Strauch, U.G., Grunwald, N., Obermeier, F., Gürster, S., and Rath, H.C. (2010). Loss of CD103+ intestinal dendritic cells during colonic inflammation. World J. Gastroenterol. *16*, 21–29.

Sun, J.B., Czerkinsky, C., and Holmgren, J. (2007). Sublingual 'oral tolerance' induction with antigen conjugated to cholera toxin B subunit generates regulatory T cells that induce apoptosis and depletion of effector T cells. Scand. J. Immunol. *66*, 278–286.

Tussiwand, R., Lee, W.L., Murphy, T.L., Mashayekhi, M., Kc, W., Albring, J.C., Satpathy, A.T., Rotondo, J.A., Edelson, B.T., Kretzer, N.M., et al. (2012). Compensatory dendritic cell development mediated by BATF-IRF interactions. Nature *490*, 502–507.

Weigmann, B., Tubbe, I., Seidel, D., Nicolaev, A., Becker, C., and Neurath, M.F. (2007). Isolation and subsequent analysis of murine lamina propria mononuclear cells from colonic tissue. Nat. Protoc. *2*, 2307–2311.

Yogev, N., Frommer, F., Lukas, D., Kautz-Neu, K., Karram, K., Ielo, D., von Stebut, E., Probst, H.C., van den Broek, M., Riethmacher, D., et al. (2012). Dendritic cells ameliorate autoimmunity in the CNS by controlling the homeostasis of PD-1 receptor(+) regulatory T cells. Immunity *37*, 264–275.

Zhang, B.Y., and Mittler, R.S. (2007). CD137 crosslinking mediates effector T cell death and immune suppression during LCMV infection. J. Immunol. *178*, LB26.

Zhang, B., Zhang, Y., Niu, L., Vella, A.T., and Mittler, R.S. (2010). Dendritic cells and Stat3 are essential for CD137-induced CD8 T cell activation-induced cell death. J. Immunol. *184*, 4770–4778.

Zheng, T., Zhang, B., Chen, C., Ma, J., Meng, D., Huang, J., Hu, R., Liu, X., Otsu, K., Liu, A.C., et al. (2018). Protein kinase p38α signaling in dendritic cells regulates colon inflammation and tumorigenesis. Proc. Natl. Acad. Sci. USA *115*, E12313–E12322.

Zlotnikov-Klionsky, Y., Nathansohn-Levi, B., Shezen, E., Rosen, C., Kagan, S., Bar-On, L., Jung, S., Shifrut, E., Reich-Zeliger, S., Friedman, N., et al. (2015). Perforin-positive dendritic cells exhibit an immuno-regulatory role in metabolic syndrome and autoimmunity. Immunity *43*, 776–787.

STAR★METHODS

KEY RESOURCES TABLE

REAGENT or RESOURCE	SOURCE	IDENTIFIER
Antibodies		
CD45 Percp	Biolegend	Cat#103130; RRID:AB_893339
CD11b BV510	Biolegend	Cat#101245; RRID:AB_2561390
F4/80 FITC	Biolegend	Cat#123108; RRID:AB_893502
Ly6G BV650	Biolegend	Cat#127641; RRID:AB_2565881
Ly6c Alexa 700	Biolegend	Cat#128024; RRID:AB_10643270
CD11c PE/cy7	Biolegend	Cat#117318; RRID:AB_493568
MHCII APC/cy7	Biolegend	Cat#107628; RRID:AB_2069377
CD103 PE	Biolegend	Cat#121406; RRID:AB_1133989
CD3 APC	Biolegend	Cat#100236; RRID:AB_2561456
CD127 PE/cy7	Biolegend	Cat#135013; RRID:AB_1937266
Sca-1 PE/cy7	Biolegend	Cat#108113; RRID:AB_493597
CD135 APC	Biolegend	Cat#135309; RRID:AB_1953264
CD115 PE	Biolegend	Cat#135506; RRID:AB_1937253
CD117 BV421	Biolegend	Cat#105827; RRID:AB_10898120
CD137 APC	Biolegend	Cat#106110; RRID:AB_2564297
CD4 BV650	Biolegend	Cat#100545; RRID:AB_11126142
CD8 BV510	Biolegend	Cat#100751; RRID:AB_2561389
IFNγ PE	Biolegend	Cat#505808; RRID:AB_315402
IL-4 PE/cy7	Biolegend	Cat#504118; RRID:AB_10898116
IL17A APC/cy7	Biolegend	Cat#506939; RRID:AB_2565780
CD64 BV421	Biolegend	Cat#139309; RRID:AB_2562694
CX3CR1 BV510	Biolegend	Cat#149025; RRID:AB_2565707
Bcl2 APC	Biolegend	Cat#633509; RRID:AB_2064149
Foxp3 PE	Biolegend	Cat#126404; RRID:AB_1089117
CCR7 PE/Dazzle 594	Biolegend	Cat#120121; RRID:AB_2564316
Helios PE/cy7	Biolegend	Cat#137235; RRID:AB_2565989
IL23 APC	BD Bioscience	Cat#565317; RRID:AB_2739178
Linage Cockail	eBioscience	Cat#22-7770-72; RRID:AB_2644066
CCR2 APC	R&D System	Cat#FAB5538A; RRID:AB_10645617
Bcl-2	Santa Cruz Biotechnology	Cat#SC-7382; RRID:AB_626736
Bcl-xL	Santa Cruz Biotechnology	Cat#SC-8392; RRID:AB_626739
Actin	Santa Cruz Biotechnology	Cat#SC-1615; RRID:AB_630835
Lamin B	Santa Cruz Biotechnology	Cat#SC-6217; RRID:AB_648158
p-NF-κB	Cell Signaling	Cat#3033S; RRID:AB_331284
Caspase-9	Cell Signaling	Cat#9504; RRID:AB_2275591
Cleaved-caspase-9	Cell Signaling	Cat#9509S; RRID:AB_2073476
p-AMPK	Cell Signaling	Cat#2537; RRID:AB_659805
AMPK	Cell Signaling	Cat#2795; RRID:AB_560856
p-TAK1	Thermo Fisher Scientific	Cat#PA5-39743; RRID:AB_2556294
TAK1	Thermo Fisher Scientific	Cat#PA5-17507; RRID:AB_10979591
ALDH1A2 (RALDH2)	Cell Signaling	Cat#83805; RRID:AB_2800032
p-p38MAPK	Cell Signaling	Cat#9211S; RRID:AB_331641
p38MAPK	Cell Signaling	Cat#9212; RRID:AB_330713

(*Continued on next page*)

Continued

REAGENT or RESOURCE	SOURCE	IDENTIFIER
SOCS3	Abcam	Cat#ab16030; RRID:AB_443287
PGC1α	Abcam	Cat#ab54481; RRID:AB_881987
E-cadherin	R&D System	Cat#AF748; RRID:AB_355568
Alexa Fluor 594 chicken anti-goat IgG	Invitrogen	Cat#A21468; RRID:AB_141859
Anti-CD16/32 FcR blocker	Biolegend	Cat#101302; RRID:AB_312801
Purified hamster anti-mouse CD3e	BD Bioscience	Cat#553058; RRID:AB_394591
Purified hamster anti-mouse CD28	BD Bioscience	Cat#553295; RRID:AB_394764
Chemicals, Peptides, and Recombinant Proteins		
CytoBox Th1 mouse	Miltenyi Biotec	Cat#130-107-761
CytoBox Th2 mouse	Miltenyi Biotec	Cat#130-107-760
CytoBox Th17 mouse	Miltenyi Biotec	Cat#130-107-758
CD4(L3T4) microbeads	Miltenyi Biotec	Cat#130-117-043
Recombinant murine IFN-r	Peprotech	Cat#315-05
Recombinant mouse IL-23 (carrier free)	Biolegend	Cat#589002; RRID:AB_10663413
Recombinant murine Flt3 lignad	Peprotech	Cat#250-31L
GM-CSF	Peprotech	Cat#315-03
Dextran sulfate sodium salt colitis grade	MP Biomedicals	Cat#101516
Lipopolysaccharides from *Escherichia coli*	Sigma	Cat#L4524
Retinoic acid	Sigma	Cat#R2625
5Z-7-oxozeaenol	Tocris	Cat#3604
AGN193109	Tocris	Cat#5758
Anti-CD137 mAb	Prof. Robert S. Mittler, Emory University	clone: 3E1
Anti-CD137L antibody	Prof. Hideo Yagita, Juntendo University	Clone: TKS-1
RBC lysis buffer	Biolegend	Cat#420301
Hematoxylin	Abcam	Cat#ab220365
Eosin	BBC Biochemical	Cat#MA0101015
EDTA	Duchefa	Cat#E0511
Dispase II	Roche	Cat#04942078001
Colagenase D	Roche	Cat#10745740001
Formaldehyde solution	Duksan	Cat#UN2209
Trizol reagent	Life Technologies	Cat#15596026
Cell activaton cocktail	Biolegend	Cat#423303
Duoset ancillary reagent kit 2	R&D System	Cat#DY008
Superscript III First-Strand Synthesis System	Invitrogen	Cat# 18080051
DTT (protease free)	Goldbio	Cat#DTT
Critical Commercial Assays		
ALDEFLUOR kit	STEMCELL TECHNOLOGY	Cat#1700
Active caspase 9 kit	Abcam	Cat#ab65615
Foxp3 stianing buffer set	eBioscience	Cat#00-5523-00
Fixation/permeabilization solution kit	BD Bioscience	Cat#554714
FITC annexin v apooptosis detection kit	BD Bioscience	Cat#556547
Fluoresbrite YG microspheres	Polysciences	Cat#17152-10
Duoset ELISA mouse IL-23	R&D System	Cat#DY1887-05
QIAamp DNA Stool Mini Kit	QIAGEN	Cat# 51504
Experimental Models: Organisms/Strains		
Mouse: *CD137*$^{-/-}$	Dr. Byoung S. Kwon, Eutilex Co, Ltd	N/A
Mouse: *CD137L*$^{-/-}$	Prof. Robert S. Mittler, Emory University	N/A

(*Continued on next page*)

Continued

REAGENT or RESOURCE	SOURCE	IDENTIFIER
Mouse: *C57BL/6J*	The Jackson Laboratory	JAX:664
Mouse: *CD137*$^{fl/fl}$	This paper	
Mouse: *CD11c*^{cre}	Prof. Hyoung-Pyo Kim Yonsei University	N/A
Mouse: *Lyz2*^{cre}	The Jackson Laboratory	JAX:4781
Mouse: *Flp*	Prof. Han-Woong Lee, Yonsei University	N/A
Mouse: *CD11c*^{cre}*CD137*$^{fl/fl}$	This paper	N/A
Mouse: *Lyz2*^{cre}*CD137*$^{fl/fl}$	This paper	N/A
Oligonucleotides		
See Table S1		N/A
Software and Algorithms		
FlowJo (version 10.0.7)	FlowJo	RRID:SCR_008520
ZEN 2012 (blue edition)	Carl Zeiss	RRID:SCR_013672
InStat (version 4.0)	GraphPad	http://www.graphpad.com/scientific-software/instat
Imeage J	Imeage J	RRID:SCR_003070

LEAD CONTACT AND MATERIALS AVAILABILITY

Further information and requests for resources and reagents should be directed to and will be fulfilled by the Lead Contact, Goo Taeg Oh (gootaeg@ewha.ac.kr). This study did not generate new unique reagents.

EXPERIMENTAL MODEL AND SUBJECT DETAILS

Animals

CD137$^{-/-}$ (Kwon et al., 2002) and *CD137L*$^{-/-}$ (DeBenedette et al., 1999) mice were crossed with *C57BL/6J* mice, and *CD137*$^{+/+}$ and *CD137L*$^{+/+}$ mice were generated as controls. CD137 (*Tnfrsf9*) floxed mice were generated from *Tnfrs9*$^{tm1a\ (EUCOMM)Wtsi}$ embryonic stem cells purchased from the European mouse mutagenesis (EUCOMM) Programme. The targeted ES cell clone was injected into 3.5-day blastocysts and transferred to the uteri of pseudopregnant foster mothers. Male chimeras were mated with *C57BL/6* females to obtain germline transmission of the *Tnfrsf9* floxed allele. *Tnfrsf9*$^{fl/fl}$ mice were generated by crossing germline-transmitted *CD137*$^{tm1a/tm1a}$ mice to *Flp* mice. To generate DC- and macrophage-specific CD137 deficient mice, *CD137*$^{fl/fl}$ mice were crossed with *CD11c*^{cre} or *Lyz2*^{cre} mice. These mice had no abnormality in weight or hematological parameters. 6-8 weeks old male littermate mice were used for *in vivo* experiments. Mice were maintained in SPF condition of a 12-h light/dark cycle, 23 ± 2°C room temperature and 55 ± 10% humidity. All animal experiments were approved by the Institutional Animal Care and Use Committees (IACUC) of Ewha Womans University and followed National Research Council Guidelines.

METHOD DETAILS

Induction of colitis and treatment

Mice were allowed to drink 2% (wt/vol) DSS (molecular weight 36–50 kDa; MP Biomedicals) dissolved in sterilized tap water to induce colitis or normal sterilized tap water as control *ad libitum* for 9 d. To examine the effect of anti-CD137 antibody (3E1) on colitis, mice were intraperitoneally injected with 3E1 (100 μg/mouse/time) on days −1, 0, +2, +4, and +6 (on day 0, mice began to drink DSS-containing water). Rat IgG was used as control.

Assessment of inflammation and histology

The severity of colitis was based on body weight loss and histopathology of the colon. Mice were weighed daily. Body weight loss was calculated as the percentage of weight lost from the baseline body weight of day 0. All mice were sacrificed 9 d after the beginning of DSS drinking and colons were harvested. Colons were divided longitudinally, swiss rolled, and fixed in 10% buffered neutralized formalin. Fixed tissues were embedded in paraffin and standard H&E staining for 5-μm colon sections was performed for histologic grading. The histological score was calculated, using a semiquantitative system for abnormalities associated with colonic tissue disruption with 0, 1, 2, 3 and 4 corresponding to no inflammation, mild inflammation, moderate inflammation, severe inflammation, and severe inflammation with necrosis, respectively (Dasgupta et al., 2014). Each histological quantification was performed in a blinded manner.

Isolation of primary cells

Intestinal LP cells were isolated, as previously described (Weigmann et al., 2007). Briefly, the intestines were removed and cut into 4- to 5-cm pieces, and feces were cleared by holding the intestine with forceps and flushing it with a syringe filled with cold PBS. The residual mesenteric fat tissues and Peyer's patches were resected, and the intestine pieces were opened longitudinally, cut into 1-cm pieces, and washed in ice-cold PBS. The pieces of intestine were incubated in 5 mL of pre-digestion solution (5 mM EDTA, 1 mM DTT in 1X HBSS without Mg^{2+} or Ca^{2+}) for 20 min at 37°C in a 50 mL tube, under slow rotation (40 *g*) in a thermal incubator. The remaining pieces were collected with a 100-μm cell strainer and incubated in fresh pre-digestion solution as described above. The above-described rotation incubation disrupted the epithelial cells from the mucosa. The remaining pieces were collected with a 100-μm cell strainer and minced with scissors into 1-mm pieces. The tissue was collected into a gentleMACS C tube [Miltenyi Biotec] containing 5 mL of digestion solution [0.05 g of collagenase D (Roche), DNase I, 0.3 g of Dispase II (Roche) in 100 mL of 1X HBSS with Mg^{2+} and Ca^{2+}] and incubated at 37°C for 30 min with a gentleMACS Dissociator (Miltenyi Biotec). Mouse spleens and lymph nodes were digested in 400 U/mL of collagenase D in FACS buffer for 25 min at 37°C on a shaker.

Immunohistochemistry

Colon tissues were fixed with 10% buffered neutralized formaldehyde and embedded in paraffin. 5-μm sections were obtained and placed on slides. Deparaffinization and dehydration of slides were done by washing slides with a series of xylene and ethanol solution. The slides were labeled with unconjugated primary goat anti-mouse E-cadherin antibody (R&D Systems) and then with Alexa 594-conjugated secondary antibodies (Invitrogen). Digital immunostaining images were captured and analyzed using an LSM780 confocal microscope (Carl Zeiss).

BMDCs

To obtain BMDCs, BM cells were harvested from femurs and tibias. RBC lysis was performed, and the remaining cells (2×10^6 cells/ml) were cultured in IMDM media (GIBCO) containing 200 ng/ml murine Flt3L (PeproTech) for 9 d (Kang et al., 2017). For the following 2 d, the DCs were induced to polarize toward $CD11b^+CD103^-$ subsets by the addition of IL-23 (1 ng/ml; PeproTech) and GM-CSF (10 ng/ml; PeproTech), or toward $CD11b^-CD103^+$ subsets by the addition of IFN-γ (0.1 ng/ml; Sigma-Aldrich) and GM-CSF (10 ng/ml) (Kang et al., 2017). For transwell co-culture experiments, $CD11b^+CD103^-$ DCs were first seeded on the bottom of 6-transwell cell culture system and pretreated with or without AGN193109 (Tocris Bioscience), a high affinity RA receptor (RAR) antagonist, and $CD11b^-CD103^+$ DCs were seeded onto the membrane of transwell cell culture inserts (pore size: 0.4 μm). After seeding, cells were stimulated with LPS (200 ng/ml; Sigma Aldrich).

Phagocytosis assay

For the analysis of phagocytosis, single-cell suspensions of colonic LP cells were incubated with 0.5 μm of Fluoresbrite YG Microspheres (Polysciences) for 70 min at 37°C. The cells were then washed twice with cold PBS, labeled with monoclonal antibodies against CD45, CD11c, MHC II, and CD11b, and analyzed by flow cytometry (BD LSRFortessa).

QUANTITATIVE REAL-TIME PCR

Total RNA was extracted with the TRIzol reagent (GIBCO) and cDNA was synthesized with a Superscript III First-Strand Synthesis System (Invitrogen). Quantitative PCR was performed using the StepOne Plus Real-Time PCR System (Applied Biosystems). To measure the bacterial DNA in the LP, DNA was isolated from faecal samples using the QIAamp DNA stool mini kit (QIAGEN) according to manufacturer's instructions. The proportion of bacterial family and genera in faecal samples were determined by real-time PCR. Quantification values were calculated by the ΔΔCT method relative to total bacterial 16S rRNA amplicons (Huang et al., 2015). Primers sequences are indicated in Table S1.

Western blot analysis

Lysates of $CD11b^+CD103^-$ DCs and $CD11b^-CD103^+$ DCs were subjected to 4%–15% gradient gel electrophoresis and the resolved proteins were transferred to PVDF membranes (Bio-Rad). The membranes were blocked for 1 h at room temperature in 5% skim milk or BSA (Bovine serum albumin) in 1X TBST, and then incubated with specific antibodies. The following antibodies were used for western blot analysis: Bcl-2 (C-21), Bcl-xL (H5), Actin (C-11), Lamin B (M20) (all from Santa Cruz Biotechnology), p-NF-κB, Caspase 9, cleaved Caspase 9, phosphorylated AMPK (p-AMPK), AMPK (all from Cell Signaling), p-TAK1, TAK1, RALDH2, phosphorylated p38MAPK (p-p38MAPK), p38MAPK (all from Thermo Fisher Scientific), SOCS3, PGC1α (both from Abcam). After washing with 1X TBST, the appropriate HRP-conjugated secondary was added for 1 h at room temperature. The bands were visualized with enhanced chemiluminescence reagents (Ab Frontier).

ELISA

The culture supernatants were assayed for IL-23 protein according to the manufacturer's instructions (R&D Systems). The cells were stimulated with LPS (200 ng/ml; Sigma Aldrich) for 24 h. The concentration of IL-23 was determined using a standard curve obtained with recombinant IL-23.

Flow cytometry

Cells were incubated with an anti-CD16/32 monoclonal antibody (BioLegend) to block the Fc receptors at 4°C for 30 min, stained with specific antibodies against surface markers in FACS buffer (PBS containing 2% FBS) at 4°C for 30 min, and washed with FACS buffer. Monitoring of apoptosis was performed by staining with anti-Annexin V antibody and PI (BD Biosciences). Cells negative for PI but positive for anti-Annexin V antibody were defined as apoptotic cells. Intracellular cytokine staining was performed using a fixation/permeabilization solution kit (BD Biosciences) or a Foxp3 staining buffer set (eBioscience). For T cell activation, cells were incubated with cell activation cocktail with Brefeldin A (BioLegend) in 1640 RPMI medium for 5 h. Stained cells were acquired using a BD LSRFortessa flow cytometer and analyzed with the FlowJo software (Tree Star).

T cell polarization assay

Naive $CD4^+$ T cells from the spleen and lymph node of 8-to-10-wk old *CD137*$^{fl/fl}$ and *CD11c*^{Cre} *CD137*$^{fl/fl}$ mice were enriched using CD4 MACS beads (130-104-453, Miltenyi Biotec) and transferred to a 96-well plate coated with anti-CD3 (5 μg/ml, eBioscience), anti-CD28 (2 μg/ml, eBioscience), and anti-CD137 antibodies (10 μg/ml). Cells were cultured for 5 d in the following T_H polarization conditions: 10 ng/ml IL-2, 10 ng/ml IL-12, and 10 μg/ml anti-IL-4 antibody for T_H1 cell polarization (CytoBox T_H1, Miltenyi Biotec); 10 ng/mL IL-4, 10 ng/mL IL-2, 10 μg/mL and anti-IFN-γ antibody for T_H2 cell polarization (CytoBox T_H2, Miltenyi Biotec); 20 ng/ml IL-6, 10 ng/ml IL-23, 10 ng/ml IL-1β, 2 ng/ml human TGF-β1, 10 μg/ml anti-IL-4 antibody, 10 μg/ml anti-IFN-γ antibody, and10 μg/ml anti-IL-2 antibody for T_H17 cell polarization (CytoBox T_H17, Miltenyi Biotec). Harvested $CD4^+$ T cells were stimulated for 5 h with cell activation cocktail with Brefeldin A (BioLegend) and intracellular cytokine staining was performed to detect intracellular INF-γ, IL-4, or IL-17A.

Statistical analysis

Unpaired Student's t test and one-way ANOVA test were performed using the InStat (version 4.0) for Windows software package (GraphPad). Shapiro–Wilk normality test was performed using the SPSS software. *P value*s less than 0.05 were considered statistically significant.

DATA AND CODE AVAILABILITY

This study did not generate any datasets.

Cell Reports, Volume *30*

Supplemental Information

CD137 Signaling Regulates Acute Colitis via RALDH2-Expressing CD11b^{-}CD103^{+} DCs

Jing Jin, In-Hyuk Jung, Shin Hye Moon, Sejin Jeon, Se-Jin Jeong, Seong-Keun Sonn, Seungwoon Seo, Mi-Ni Lee, Eun Ju Song, Hyae Yon Kweon, Sinai Kim, Tae Kyeong Kim, Juyang Kim, Hong Rae Cho, Jae-Hoon Choi, Byungsuk Kwon, and Goo Taeg Oh

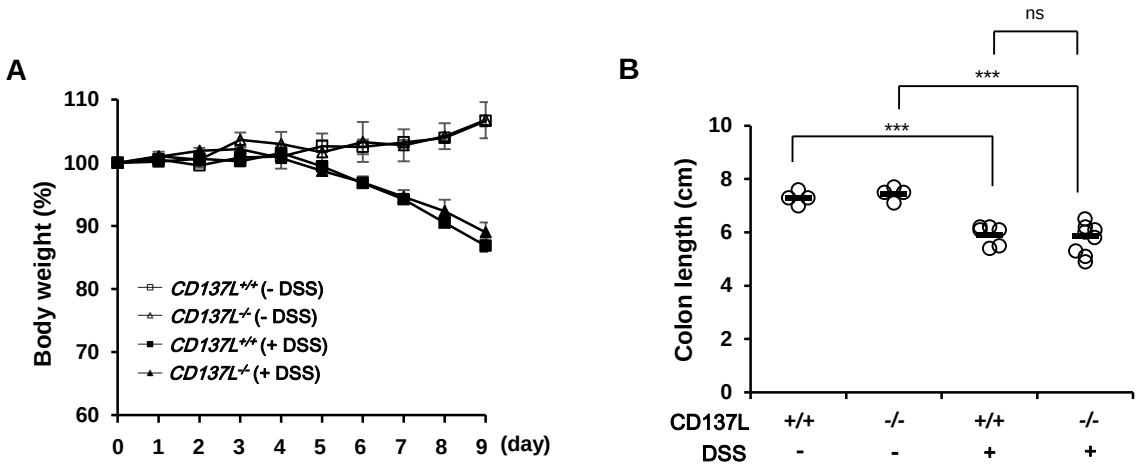

Figure S1. *CD137L*$^{-/-}$ mice show a similar degree of colitis severity to WT mice, related to Figure 1

(A) Body weight changes of *CD137L*$^{+/+}$ (noncolitic, n = 4), *CD137L*$^{-/-}$ (noncolitic, n = 4), *CD137L*$^{+/+}$ (colitic, n = 6), and *CD137L*$^{-/-}$ mice (colitic, n = 8). Data were presented as mean ± SEM.

(B) Colon length of *CD137L*$^{+/+}$ (noncolitic, n = 4), *CD137L*$^{-/-}$ (noncolitic, n = 4), *CD137L*$^{+/+}$ (colitic, n = 6), and *CD137L*$^{-/-}$ mice (colitic, n = 8) . ***$P < 0.001$ (Student's t test).

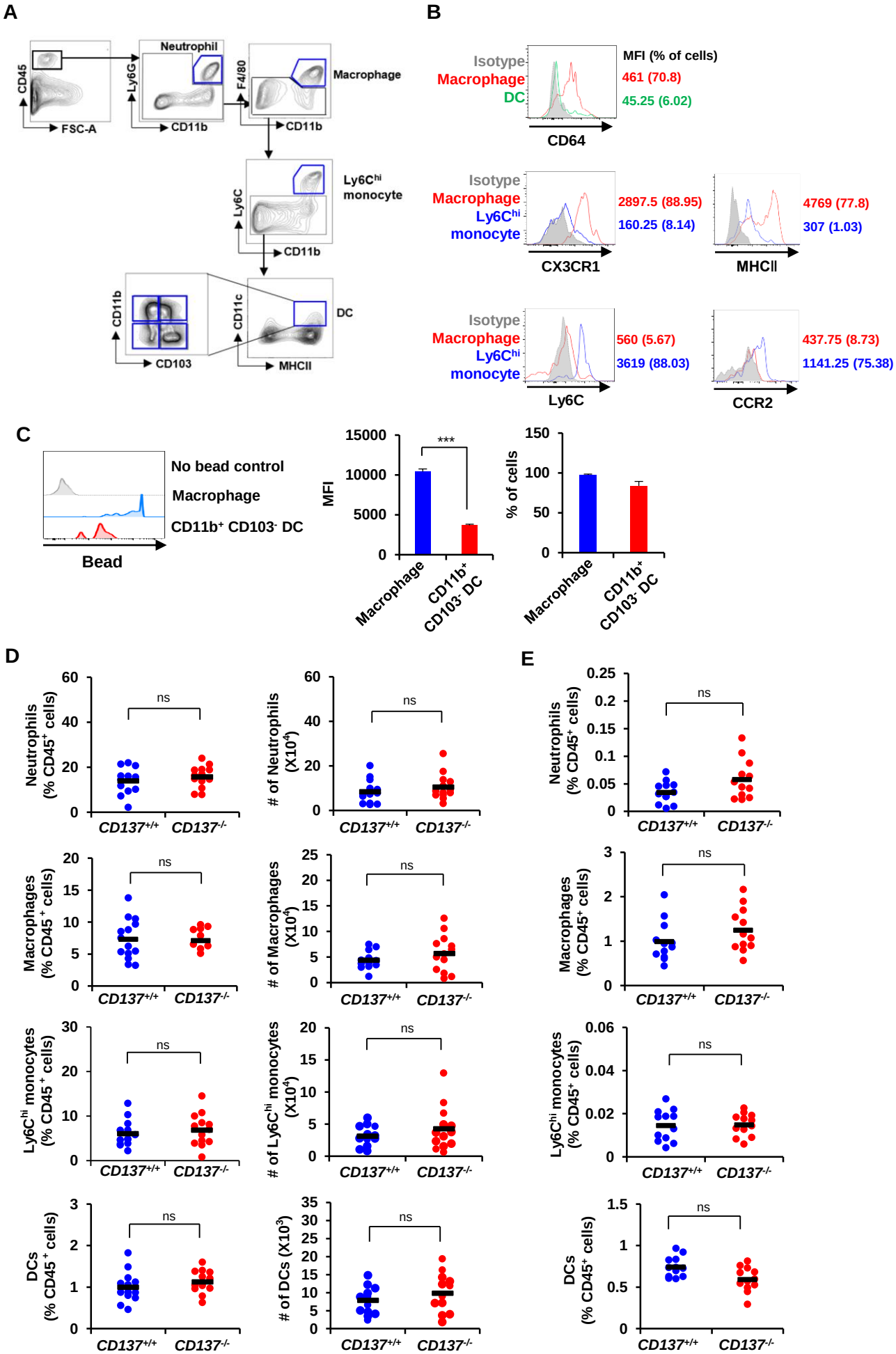
A
CD45
FSC-A
Ly6G
Neutrophil
CD11b
F4/80
Macrophage
CD11b
Ly6C
Ly6C^hi monocyte
CD11b
CD11b
CD103
CD11c
MHCII
DC
B
Isotype
Macrophage
DC
MFI (% of cells)
461 (70.8)
45.25 (6.02)
CD64
Isotype
Macrophage
Ly6C^hi monocyte
2897.5 (88.95)
160.25 (8.14)
CX3CR1
4769 (77.8)
307 (1.03)
MHCII
Isotype
Macrophage
Ly6C^hi monocyte
560 (5.67)
3619 (88.03)
Ly6C
437.75 (8.73)
1141.25 (75.38)
CCR2
C
No bead control
Macrophage
CD11b+ CD103- DC
Bead
MFI
***
% of cells
Macrophage
CD11b+ CD103- DC
D
E
Neutrophils (% CD45+ cells)
# of Neutrophils (X10^4)
Macrophages (% CD45+ cells)
# of Macrophages (X10^4)
Ly6C^hi monocytes (% CD45+ cells)
# of Ly6C^hi monocytes (X10^4)
DCs (% CD45+ cells)
# of DCs (X10^3)
ns
CD137+/+
CD137-/-

Figure S2. Analysis of myeloid cells in the LP and MLNs, related to Figure 2.

(A) Gating strategies of LP myeloid cell types.

(B) Flow cytometric analysis for cell surface marker expression of LP macrophages (red lines), Ly6c^{hi} monocytes (blue lines), and DCs (green lines).

(C) Analysis for the phagocytic activities of LP macrophages and CD11b^{+}CD103^{-} DCs. Data were presented as mean ± SEM of two independent experiments. ***$P < 0.001$ (Student's t test).

(D and E) Flow cytometric analysis for the immune cell compositions in the LP (D) and MLNs (E) of colitic *CD137*$^{+/+}$ (n =13 in LP; n = 12 in MLN) or *CD137*$^{-/-}$ mice (n =13 in LP; n = 12 in MLN).

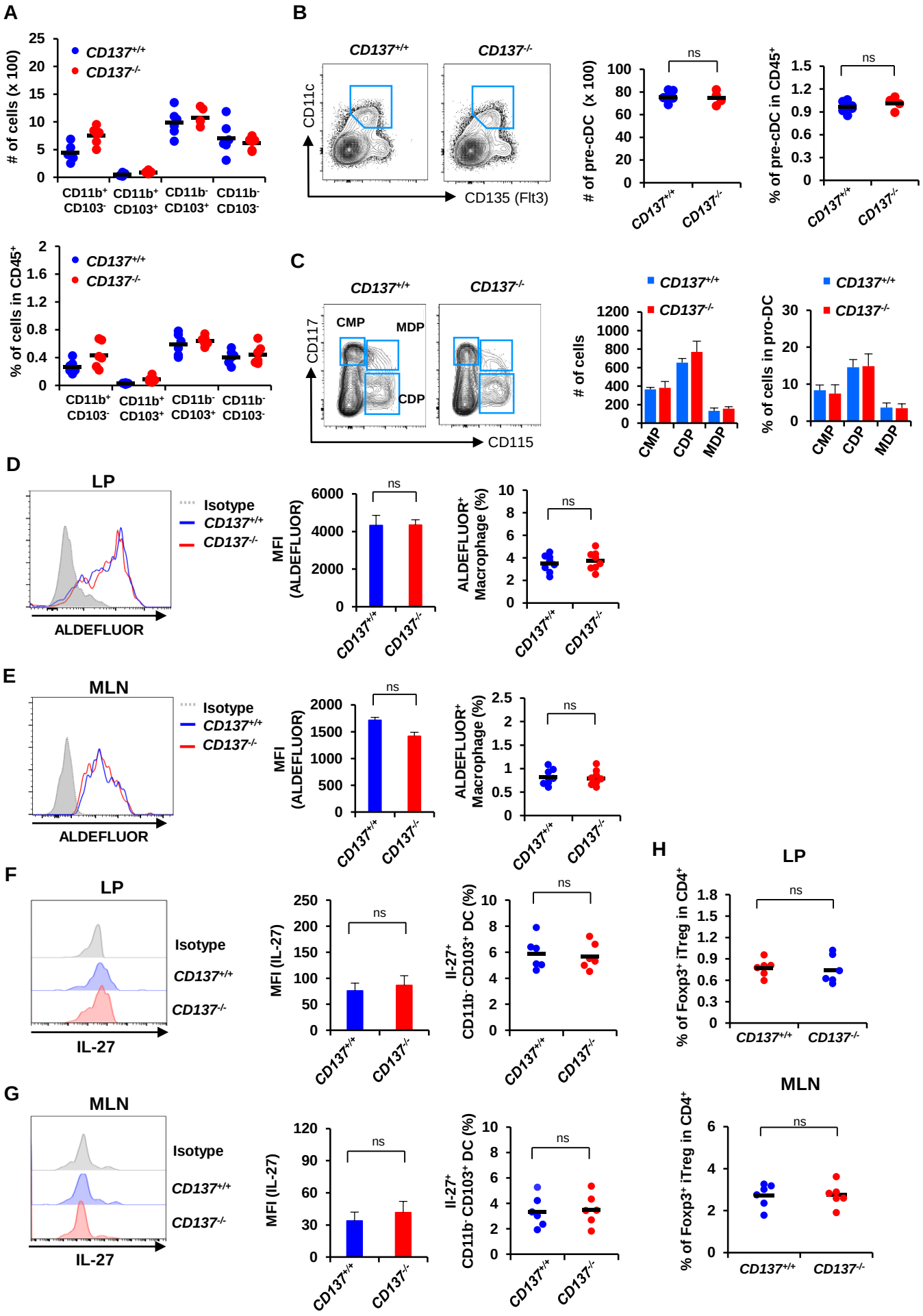
A
# of cells (x 100)
CD137+/+
CD137-/-
CD11b+ CD103-
CD11b+ CD103+
CD11b- CD103+
CD11b- CD103-
% of cells in CD45+
B
CD137+/+
CD137-/-
CD11c
CD135 (Flt3)
# of pre-cDC (x 100)
% of pre-cDC in CD45+
ns
C
CD117
CMP
MDP
CDP
CD115
# of cells
% of cells in pro-DC
D
LP
Isotype
ALDEFLUOR
MFI (ALDEFLUOR)
ALDEFLUOR+ Macrophage (%)
E
MLN
F
IL-27
MFI (IL-27)
Il-27+ CD11b- CD103+ DC (%)
G
H
% of Foxp3+ iTreg in CD4+

Figure S3. FACS analysis of intestinal macrophages and DC subsets, and BM cDC progenitors/precursors, related to Figure 2.

(A) Flow cytometric analysis for LP DC subsets of *CD137*$^{+/+}$ (n = 6) and *CD137*$^{-/-}$ mice (n = 6).

(B) Flow cytometric analysis for BM pre-DCs of *CD137*$^{+/+}$ (n = 6) and *CD137*$^{-/-}$ mice (n = 6).

(C) Flow cytometric analysis for BM DC progenitors of *CD137*$^{+/+}$ (n = 6) and *CD137*$^{-/-}$ mice (n = 6).

(D and E) Flow cytometric analysis for ALDEFLUOR staining in LP (D) and MLN macrophages (E) of colitic *CD137*$^{+/+}$ (n = 8) and *CD137*$^{-/-}$ mice (n = 8). Data were presented as mean ± SEM.

(F and G) Flow cytometric analysis for intracellular IL-27 in LP (F) and MLN $CD3^+CD4^+Foxp3^+Helios^-$ inducible Treg (iTreg) cells (G) of colitic *CD137*$^{+/+}$ (n = 6) and *CD137*$^{-/-}$ mice (n = 6). Data were presented as mean ± SEM.

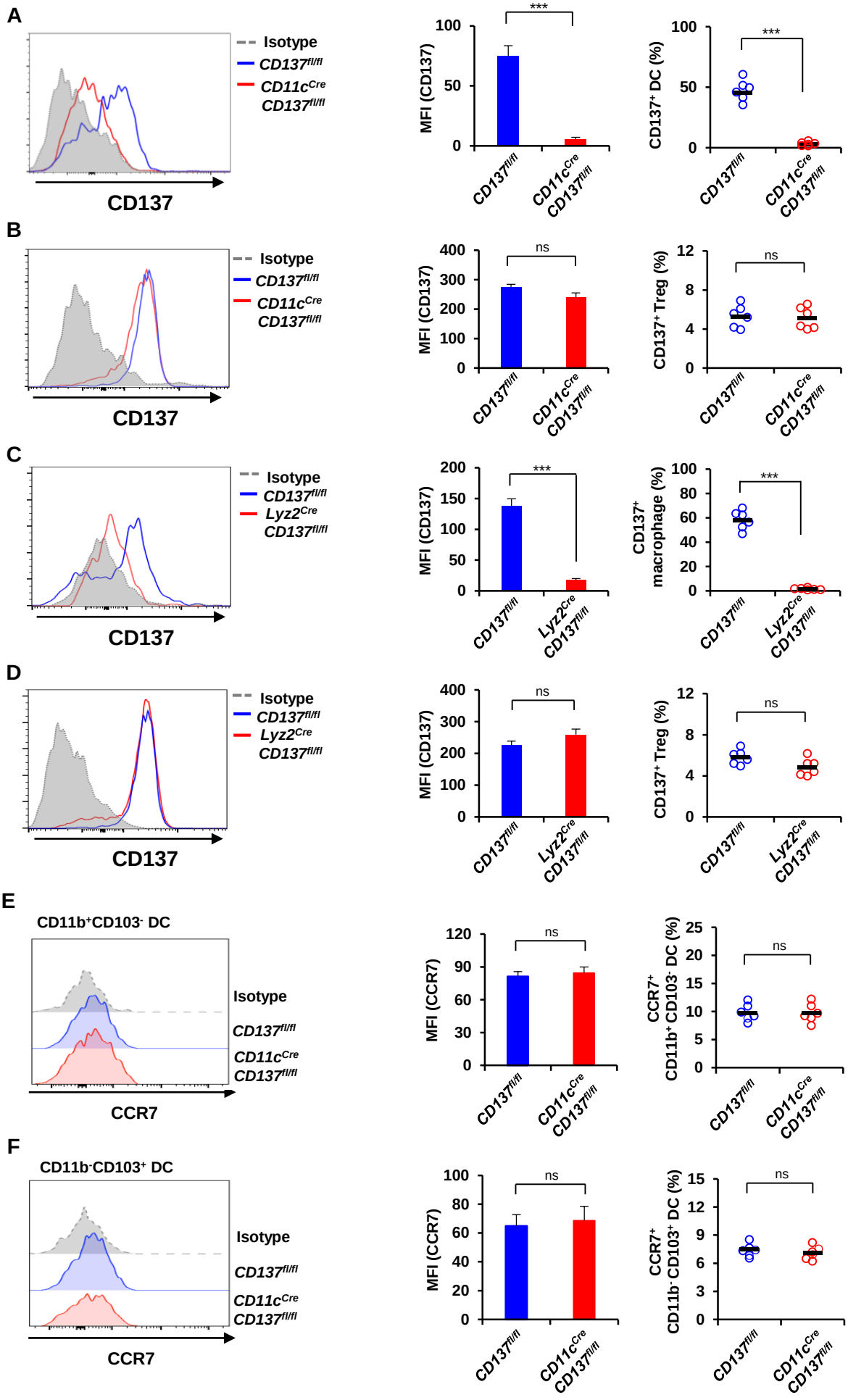
A
Isotype
CD137fl/fl
CD11cCre CD137fl/fl
CD137
MFI (CD137)
***
CD137+ DC (%)
***
B
Isotype
CD137fl/fl
CD11cCre CD137fl/fl
CD137
MFI (CD137)
ns
CD137+ Treg (%)
ns
C
Isotype
CD137fl/fl
Lyz2Cre CD137fl/fl
CD137
MFI (CD137)
***
CD137+ macrophage (%)
***
D
Isotype
CD137fl/fl
Lyz2Cre CD137fl/fl
CD137
MFI (CD137)
ns
CD137+ Treg (%)
ns
E
CD11b+CD103- DC
Isotype
CD137fl/fl
CD11cCre CD137fl/fl
CCR7
MFI (CCR7)
ns
CCR7+ CD11b+CD103- DC (%)
ns
F
CD11b-CD103+ DC
Isotype
CD137fl/fl
CD11cCre CD137fl/fl
CCR7
MFI (CCR7)
ns
CCR7+ CD11b-CD103+ DC (%)
ns

Figure S4. FACS analysis of CD137 and CCR7 expression in intestinal DCs , related to Figure 3.

(A and B) Flow cytometric analysis for CD137 expression in LP DCs (A) and Treg cells (B) of *CD137*$^{fl/fl}$ (n = 6 each group) and *CD11c*^{cre}*CD137*$^{fl/fl}$ mice (n = 6 each group). Data were presented as mean ± SEM. ***$P < 0.001$ (Student's t test).

(C and D) Flow cytometric analysis for CD137 expression in LP macrophages (C) and Treg cells (D) of *CD137*$^{fl/fl}$ (n = 6 each group) and *Lyz*^{cre}*CD137*$^{fl/fl}$ mice (n = 6 each group). Data were presented as mean ± SEM. ***$P < 0.001$ (Student's t test).

(E and F) Flow cytometric analysis for CCR7 expression in LP CD11b^{+}CD103^{-} (E) and CD11b^{-}CD103^{+} DCs (F) of *CD137*$^{fl/fl}$ (n = 6 each group) and *CD11c*^{cre}*CD137*$^{fl/fl}$ mice (n = 6 each group). Data were presented as mean ± SEM.

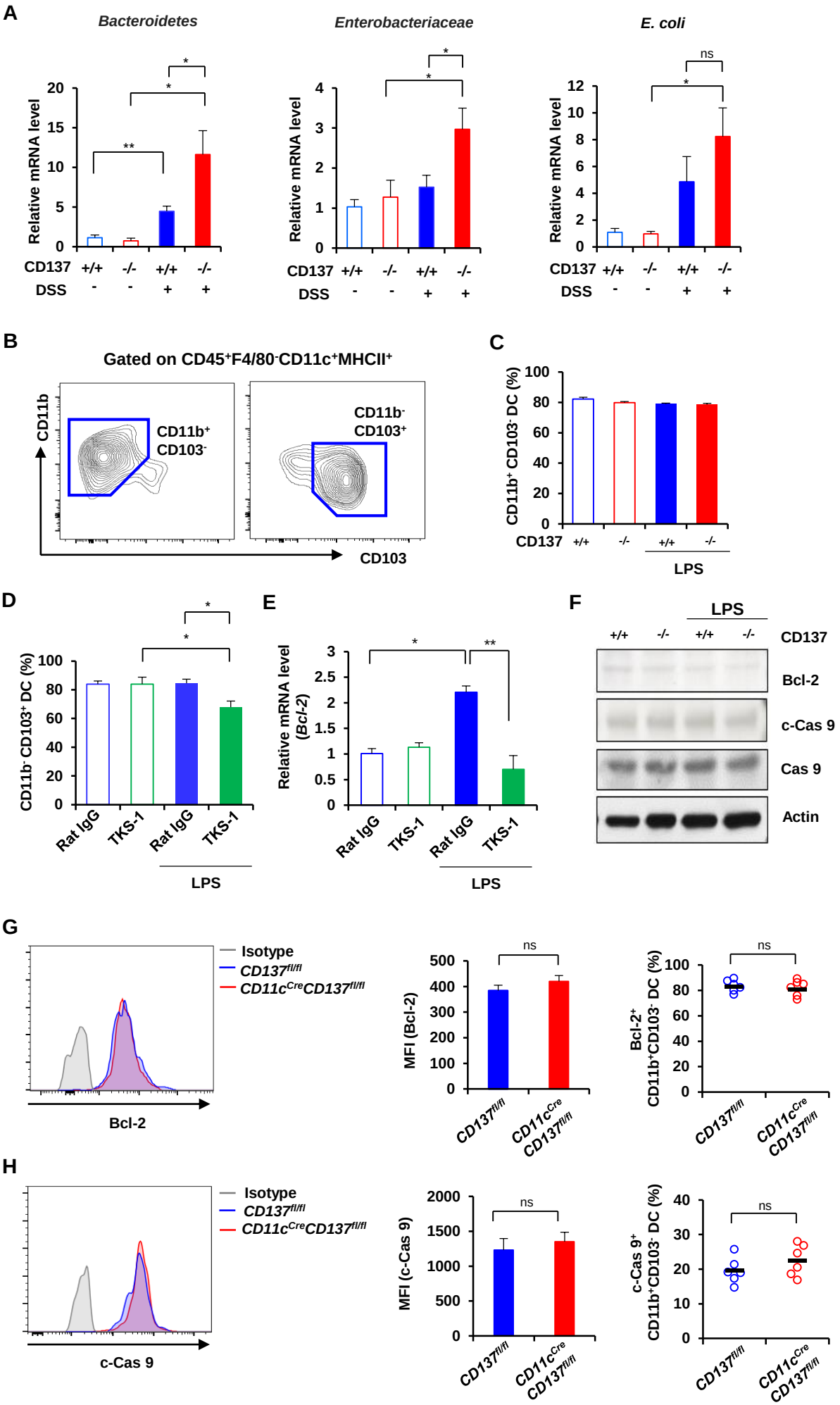
A
Bacteroidetes
Enterobacteriaceae
E. coli
Relative mRNA level
CD137 +/+ -/- +/+ -/-
DSS - - + +
ns
B
Gated on CD45+F4/80-CD11c+MHCII+
CD11b
CD11b+ CD103-
CD11b- CD103+
CD103
C
CD11b+ CD103- DC (%)
CD137 +/+ -/- +/+ -/-
LPS
D
CD11b- CD103+ DC (%)
Rat IgG TKS-1 Rat IgG TKS-1
LPS
E
Relative mRNA level (Bcl-2)
Rat IgG TKS-1 Rat IgG TKS-1
LPS
F
LPS
+/+ -/- +/+ -/-
CD137
Bcl-2
c-Cas 9
Cas 9
Actin
G
Isotype
CD137fl/fl
CD11cCreCD137fl/fl
Bcl-2
MFI (Bcl-2)
CD137fl/fl
CD11cCre CD137fl/fl
Bcl-2+ CD11b+CD103- DC (%)
H
Isotype
CD137fl/fl
CD11cCreCD137fl/fl
c-Cas 9
MFI (c-Cas 9)
c-Cas 9+ CD11b+CD103- DC (%)

Figure S5. Penetration of gut bacterial microbiota and effects of LPS on intestinal DC survival, related to Figure 4.

(A) Analysis for bacterial penetration into the colon in *CD137*$^{+/+}$ (noncolitic, n = 3), *CD137*$^{-/-}$ (noncolitic, n = 3), *CD137*$^{+/+}$ (colitic, n = 3), and *CD137*$^{-/-}$ mice (colitic, n =3). PCR analysis of 16S rDNA. Data were presented as mean ± SEM. **P* < 0.05 (Student's t test).

(B) Representative FACS dot plots for polarized CD11b^{+}CD103^{-} and CD11b^{-}CD103^{+} BMDCs gated from CD45^{+}F4/80^{-}CD11c^{+}MHCII^{+} cells.

(C) Portions of polarized CD11b^{+}CD103^{-} DCs in *CD137*$^{+/+}$ and *CD137*$^{-/-}$ BMDCs after stimulation with LPS for 24 h. Data were presented as mean ± SEM of three independent experiments.

(D) Portions of polarized CD11b^{-}CD103^{+} DCs in *CD137*$^{+/+}$ BMDCs after stimulation with LPS in the presence of anti-CD137L antibody (TSK-1) for 24 h. Data were presented as mean ± SEM of three independent experiments. **P* < 0.05 (Student's t test).

(E) RT-PCR analysis for *Bcl-2* expression in of polarized *CD137*$^{+/+}$ CD11b^{-}CD103^{+} BMDCs after stimulation with LPS in the presence of anti-CD137L antibody (TSK-1) for 12 h. Data were presented as mean ± SEM of three independent experiments. **P* < 0.05 (Student's t test).

(F) Western blot analysis of Bcl-2, caspase 9, and cleaved Caspase 9 (c-Cas 9) in polarized *CD137*$^{+/+}$ and *CD137*$^{-/-}$ CD11b^{+}CD103^{-} BMDCs after stimulated with LPS for 24 h.

(G and H) Flow cytometric analysis for intracellular Bcl-2 (G) and cleaved Caspase 9 (H) expression in LP CD11b^{+}CD103^{-} DCs of colitic *CD137*$^{fl/fl}$ (n = 6) and colitic *CD11c*^{cre}*CD137*$^{fl/fl}$ mice (n = 6). Data were presented as mean ± SEM.

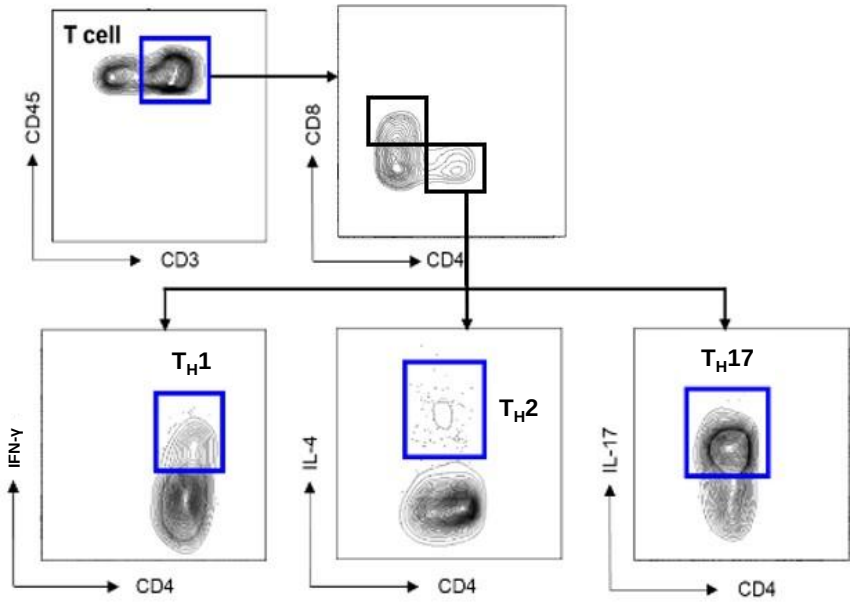

Figure S6. Gating strategies for T cell subsets, related to Figure 6.

After SSC^{low} and FSC^{low} dead cells, doublet cells, and autofluorescent cells were gated out, T_H1 cells were gated as $CD45^+CD3^+CD4^+IFN\text{-}\gamma^+$, T_H2 cells were gated as $CD45^+CD3^+CD4^+IL\text{-}4^+$, and T_H17 cells were gated as $CD45^+CD3^+CD4^+IL\text{-}17^+$.

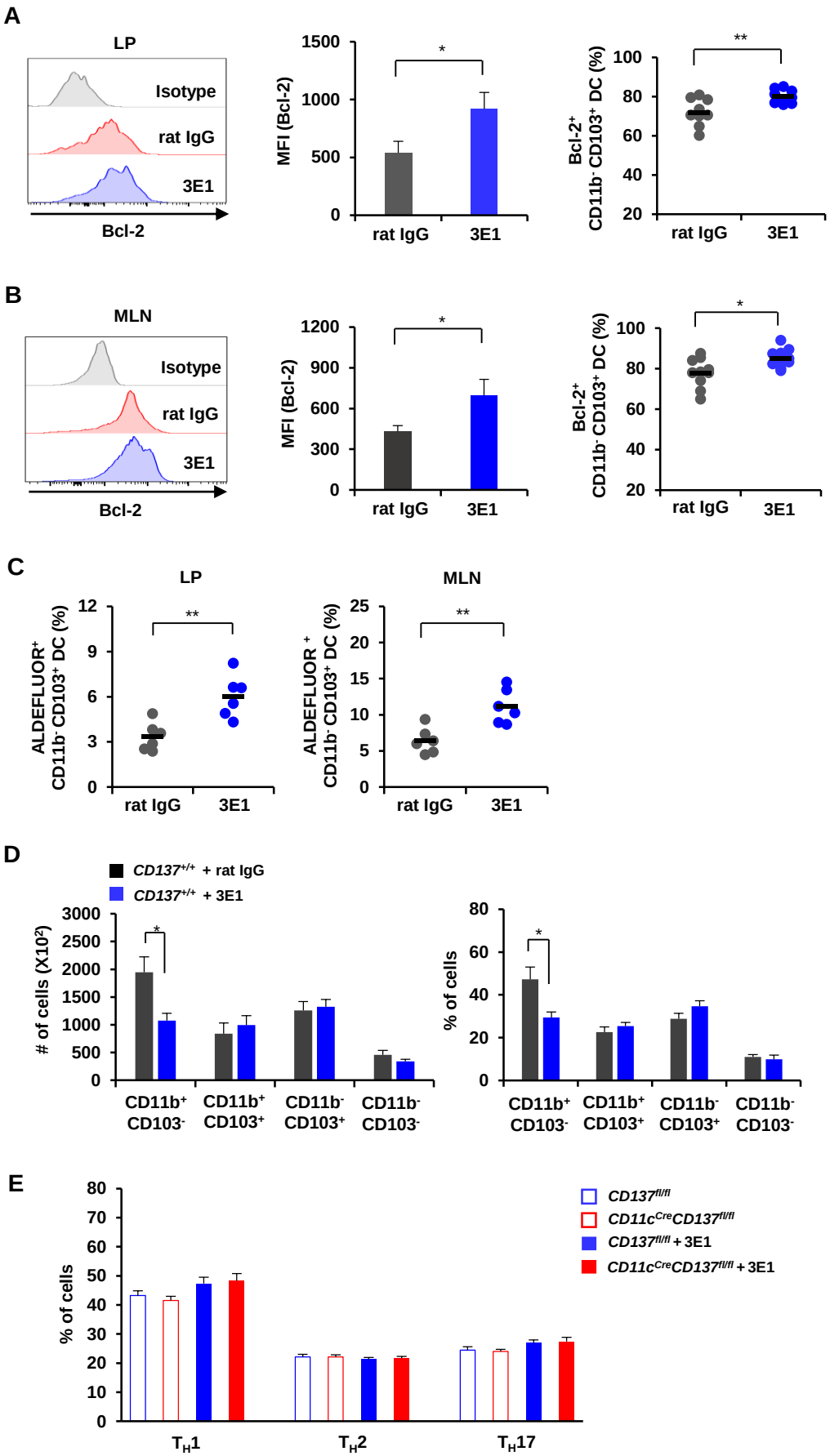
A
LP
Isotype
rat IgG
3E1
Bcl-2
MFI (Bcl-2)
rat IgG
3E1
Bcl-2+ CD11b- CD103+ DC (%)
B
MLN
C
LP
MLN
ALDEFLUOR+ CD11b- CD103+ DC (%)
D
CD137+/+ + rat IgG
CD137+/+ + 3E1
# of cells (X10²)
% of cells
CD11b+ CD103-
CD11b+ CD103+
CD11b- CD103+
CD11b- CD103-
E
CD137fl/fl
CD11cCreCD137fl/fl
CD137fl/fl + 3E1
CD11cCreCD137fl/fl + 3E1
TH1
TH2
TH17

Figure S7. Injection of 3E1 increases Bcl-2 expression and RADH2 activities in intestinal CD11b^{-}CD103^{+} DCs, related to Figure 7.

(A and B) Flow cytometric analysis for intracellular Bcl-2 in LP (A) and MLN (B) CD1b^{-}CD103^{+} DCs of colitic *CD137*$^{+/+}$ mice injected with 3E1 (n = 9 in LP; n = 10 in MLN) or rat IgG (n = 9 in LP; n = 10 in MLN). **P* < 0.05; ***P* < 0.01 (Student's t test).

(C) Flow cytometric analysis for ALDEFLUOR staining in LP and MLN CD11b^{-}CD103^{+} DCs of colitic *CD137*$^{+/+}$ mice injected with 3E1 (n = 6 each group) or rat IgG (n = 6 each group). ***P* < 0.01 (Student's t test).

(D) Flow cytometric analysis for LP DC subsets of absolute numbers (*left*) and percentages (*right*) of DC subsets of colitic *CD137*$^{+/+}$ mice injected with 3E1 (n = 6) or rat IgG (n = 6). Data were presented as mean ± SEM. **P* < 0.05 (Student's t test).

(E) Analysis for T_H polarization of *CD137*$^{fl/fl}$ and *CD11c*^{Cre}*CD137*$^{fl/fl}$ CD4^{+} T cells under T_H polarization conditions in the presence of 3E1 (n = 4 each group) or rat IgG (n = 4 each group) for 5 d. T_H1, IFN-γ^{+}CD4^{+}; T_H2, IL-4^{+}CD4^{+}; T_H17, IL-17^{+}CD4^{+}. Data were presented as mean ± SEM.